Influence of the Indian Ocean Subtropical Dipole on the Agulhas Current

Mthetho Vuyo Sovara
SVRMTH001

Supervisors: Juliet Hermes, Chris Reason

Submitted in partial fulfillment of the requirements for the degree of Master of Science (Ocean and Climate Dynamics)

Department of Oceanography
Faculty of Science
University of Cape Town
Rondebosch
Cape Town
7701

February 2014

PLAGIARISM DECLARATION

1. I know that plagiarism is wrong. Plagiarism is using another's work and to pretend that it is one's own.

2. I have used the Harvard style of referencing as the convention for citation and referencing. Each significant contribution to, and quotation, in this essay/report/project from the work, or works of other people has been cited and referenced.

3. This Mini-dissertation is my own work.

SIGNATURE: _____

DATE: _____

Abstract

Modern studies have successfully linked Subtropical Dipole (SIOD) events to southern Africa's austral summer precipitation patterns, however, none have investigated the SIOD's influence on the Greater Agulhas Current System. Here, the SIOD climatology was developed using a Regional Ocean Modeling System (ROMS) configured with GFDL-CORE v.2b reanalysis winds and heat fluxes for the 1958-2007 period. This configuration allows for a relatively accurate spatial and temporal account of the Sea Surface Temperature (SST) and Sea Surface Height (SSH) variability in the Subtropical Indian Ocean (SIO). Simulation and evaluation of SIOD events was achieved through the application of the Empirical Orthogonal Function (EOF), Wavelet Analysis and Composite Map Analysis. The EOF applied to monthly SST anomalies for the months January to December during the years 1958-2007 in the SIO resulted in the SIOD phenomenon emerging as the second EOF mode and explaining 8.93% of the total variance of the SIO. Moreover, the EOF applied only to the austral summer (JFM) months emerges the SIOD as the first EOF mode and explaining 20.84% of the total variance in the SIO. ROMS model results and statistical correlation results suggest that SIOD SST variability is neither linked to the El Nino-Southern Oscillation (ENSO) nor the Tropical Indian Ocean Dipole (IOD) phenomena, notwithstanding that SIOD events have in the past, coincided with some El Nino and La Nina events. Composite map analysis results suggest no significant influence of SIOD events on anomalous Agulhas Current SST and SSH during positive and negative SIOD years. Examination of lagged statistical correlations also showed no significant relationship between the anomalous SIOD index and the satellite derived geostrophic velocity at the core of the Agulhas Current for the period 1993-2007.

Acknowledgements

This work would have not been possible without the most valued input from my supervisors Dr. Juliet Hermes (SAEON) and Professor Chris Reason (UCT). They showed vast amounts of patience and fortitude throughout the course of the project for which I am very grateful. Acknowledgments are due to Dr. Julie Deshayes (IRD/ICEMASA) for all her invaluable scientific input throughout the course of this study. It was a great honour and pleasure working with a scientist of her caliber.

Gratitude is also due to Mr. soon to be Dr. Ben Loveday (UCT) for providing the ROMS model data and Dr. Marjolaine Krug (CSIR) for providing the Agulhas Current satellite data. Vincent Guri (Ingenieur, SHT) and Dr. Issufo Halo (UCT), I am forever grateful for assistance with the model simulations in Matlab. I learn a lot of programming skills from these two gentlemen.

I would like to thank the Department of Environmental Affairs, the National Research Foundation, UCT Alumini in the United Kingdom and the Department of Oceanography for their financial assistance towards this project.

Acknowledgments are also due to the Department of Oceanography's administrator Mrs Claire Khai and the Librarian Mrs. Nadia Jabaar, together with and the Senior Scientific Officer Mr. Raymond Roman for always willing to help in the best possible way. To my colleagues, Ms. Kolisa Sinyanya, Ms. Penny Driver and Dr. Yonss Jose, Hayley Evers-King I am forever grateful for all your support. I would also like to thank my parents Mathemba and Nomawethu Sovara for their support.

This work is living proof that freedom fighters like the Late Nelson Rolihlahla Mandela and Steve Biko did not waster the time and lives fighting for a non-worthy cause. I hope I have made them proud.

Table of Contents

1. Introduction 10

2. Literature Review 12

2.1 The Indian Ocean Subtropical Dipole (SIOD) 12

2.2 Subtropical Indian Ocean Dipole Events 16

2.3 The Agulhas Current 17

3. Materials and Methods 21

3.1 Model Overview 21

3.2 Empirical Orthogonal Function (EOF) 23

3.3 Satellite alitmetry observations of the Agulhas Current 25

3.4 Spectral Analysis 27

3.5 Wavelet Analysis 27

3.6 Observational SIOD Index 28

3.7 The ENSO Index 28

3.8 The IOD Index 28

3.9 NCEP-NCAR reanalysis data 29

3.10 Modern Era-Retrospective Analysis for Research and Applications (MERRA) 29

3.11 Composite Map Analysis 30

4. Results 32

4.1 Introduction 32

4.2 Model validation & climatology 33

4.3 NE and SW IO SST anomaly patterns 37

4.4 SST variability in the NE IO 38

4.5 SST variability in the SW IO 39

4.6 EOF Analysis of the subtropical Indian Ocean ……41

4.7 EOF PC2 component and ROMS SIOD Index analysis……43

4.8 Wavelet analysis of the observed SIOD index……47

4.9 SIOD Composite Map Analysis 49

4.10 SIOD event years in the Agulhas Region during the austral summer ……56

4.11 Jason/Topex track #020 geostrophic velocity of the Agulhas Current ……..62

4.12 Statistical correlations between climate modes and the Agulhas Current ……63

4.13 Precipitation correlations..... 68

5. Discussion..... 70

5.1 Subtropical Indian Ocean variability..... 70

5.2 EOF Analysis 71

5.3 Agulhas Current Composites..... 72

5.4 Correlations 73

6. Conclusion 75

7. References 77

List of Figures and Tables

Figures:

Chapter 2

Figure 1: Upper panel; Correlation between rainfall anomalies for the period 1979-98 and the corresponding time series of SDI. Values exceeding 99% of confidence limit (with a two-tailed t test) are shaded. Lower panel; The composite of moisture divergence in February for six SIOD events (see Behera and Yamagata, 2001). 13

Figure 2: A schematic of the greater Agulhas Current System. 18

Chapter 3

Figure 3: ROMS domain showing SST climatology and poles (blue) where SIOD index has been computed and Agulhas Current region (green) where anomalous SST and SSH has been assessed for a correlation to the SIOD phenomena. 23

Figure 4: SST maps obtained (a) from 5-day weighted averages centered on the 29th of March 2010 and (b) during the passage of a large offshore meander on the 18th of May 2010. Arrows show the geostrophic currents along Topex-Jason Track #020, offshore Port Elizabeth. The Agulhas Current flow is associated with local SST maximum and strong. 26

Chapter 4

Figure 5: World Ocean Atlas (2009) monthly SST climatological mean in the Indian Ocean based on the period 1958-2007 showing the 28^0 isotherm. 35

Figure 6: ROMS monthly SST climatological mean in the Indian Ocean based on the period 1958-2007 also showing 28^0 isotherm. 36

Figure 7: ROMS SST anomalies for the eastern subtropical pole (55^0E-65^0E, 37^0S-27^0S) and western subtropical pole (90^0E-100^0E, 28^0S-18^0S) of the subtropical Indian Ocean basin for the period 1958-2007. 37

Figure 8: (a) The normalized time-series of the ROMS SST anomalies for the NE IO pole of the subtropical Indian Ocean, (b) wavelet spectrum for the period 1958-2007, alongside (c) the global power spectrum. The white contours represent the 95% significance regions. The cone-of-influence is represented by the dotted black line and it represents the region of the wavelet spectrum where the edge effects become important. In cases where the end-points are unimportant, the COI can be disregarded (Meyers *et al*., 1993). 39

Figure 9: Same as Figure 8 but for the western Indian Ocean region. 40

Figure 10: EOF analysis applied on ROMS monthly SST anomalies. EOF spatial patterns (a, b and c) and time series (d, e and f) for the first, second and third EOF mode of monthly SST anomalies for the period 1958 to 2007 in the subtropical Indian Ocean. 42

Figure 11: EOF analysis applied on ROMS monthly SST anomalies. EOF spatial pattern (a, b and c) and time series (d, e and f) for the first, second and third EOF mode of JFM SST anomalies for the period 1958 to 2007 in the subtropical Indian Ocean. 43

Figure 12: (a) Wavelet analysis applied on the ROMS monthly (all months) PC2 component of the 2nd EOF mode of the subtropical Indian Ocean (10^0S-45^0S, 40^0E-110^0E), (b) wavelet spectrum for the period 1958-2007, alongside (c) the global power spectrum. 45

Figure 13: (a) The normalized time-series of ROMS IOSD computed from SST anomaly difference between western (55^0E-65^0E, 37^0S-37^0S) and eastern (90^0E-100^0E, 28^0S-18^0S) subtropical Indian Ocean. 46

Figure 14: SIOD index calculated from ROMS (black), observations (red), and the model EOF PC2 component time series (blue). These normalized indices describe the inter-annual SST variability in the subtropical Indian Ocean basin for the period 1958-2007. 47

Figure 15: Anomaly difference computed from the same region as figure 12 & 13 but represents data from the observational dataset of Behera & Yamagata (2001). 48

Figure 16: ROMS anomalous SST prior positive SIOD event years. The boxes in blue denote the regions where the SST used to derive the SIOD index was taken. 51

Figure 17: ROMS anomalous SST prior negative SIOD event years. The boxes in blue denote the regions where the SST used to derive the SIOD index was taken. 52

Figure 18: ROMS anomalous SST during composite positive SIOD event years (listed above). Positive SIOD event years are characterized by cool SST anomalies found elongated obliquely from the eastern subtropical region to the western tropical region and warm SST anomalies in the southeastern region of the southern Indian Ocean. The boxes in blue denote the regions where the SST used to derive the SIOD index was taken. 53

Figure 19: ROMS anomalous SST during composite negative SIOD event years (listed above). Negative SIOD event years are characterized by warm SST anomalies found elongated obliquely from the eastern subtropical region to the western tropical region and cool SST anomalies in the southeastern region of the southern Indian Ocean. The boxes in blue denote the regions where the SST used to derive the SIOD index was taken. 54

Figure 20: ROMS anomalous SST composite difference maps (Positive modes – Negative modes) for the period 1958-2007. The boxes in blue denote the regions where the SST used to derive the SIOD index was taken. 55

Figure 21: A zoom of model JFM SST anomalies with mean SST contours (^{0}C) during positive (a) and negative (b) SIOD events. 59

Figure 22: A zoom of the model JFM SIOD SST composite difference with mean SST contours (^{0}C). 60

Figure 23: A zoom of model JFM SSH anomalies with the mean SSH contours (m) during positive (a) and negative (b) SIOD events. 61

Figure 24: A zoom of the model JFM SIOD SSH composite difference with mean SSH contours (m). 62

Figure 24: (a) Amplitude of the Gaussian fit to the Agulhas Current core velocities derived from the 10-day along-track altimetry (in grey). Overlaid in black are the corresponding monthly averages. (b) Continuous wavelet transform of the Gaussian fit amplitudes, with black contour lines indicating the 95% confidence interval. (c) Power frequency spectra for the Gaussian fit

amplitudes, the dashed red lines indicates the 95% confidence level. (d) Monthly seasonal variations of the Gaussian amplitudes with the climatology plotted as a thick red line. Figure taken from Krug & Tournadre (2012). 63

Figure 25: Anomalous ENSO index (black) and the anomalous ROMS SIOD index (red) both from 1958-2007. 65

Figure 26: Anomalous ROMS SIOD index (black) and the anomalous IOD index (red) both from 1958-2007. 65

Figure 27: Anomalous ROMS SIOD index (black) and the anomalous geostrophic velocity at the core of the Agulhas Current (red) both from 1993-2007. 66

Figure 28: 12 month average NASA MERRA reanalysis latent heat flux anomalies (1979-2007) correlated to them ROMS model SIOD index at 0 lag. 69

Figure 29: 12 month average NCEP-NCAR twentieth century reanalysis precipitation anomalies (1979-2007) correlated to them ROMS model SIOD index at 0 lag. 69

Tables:

Chapter 2

Table 1: List of years when positive (negative) dipole events occurred in the South Indian Ocean, Hermes & Reason (2005). 17

Chapter 4

Table 2: R-values of correlations between ENSO, IOD, SIOD, the second EOF PC2, geostrophic velocity at the core of the Agulhas Current, Agulhas Current SST and Agulhas Current SSH with a 0 – 12 month lag. 66

Table 3: R-values of correlations between the IOD, ROMS SIOD, the second EOF PC2 component, geostrophic velocity at the core of the Agulhas Current, Agulhas Current SST and Agulhas Current SSH with a 0 – 12 month lag. 67

Table 4: R-values of correlations between the ROMS SIOD, second EOF PC2 component, geostrophic velocity at the core of the Agulhas Current, Agulhas Current SST and Agulhas Current SSH with a 0 – 12 month lag. 67

1. Introduction

There have been numerous observational and model studies over the past 15 years aimed at successfully defining and linking SIOD events to weather and climate (Reason, 2001, 2002). Behera & Yamagata (2001) revealed that SIOD events are coupled atmospheric/ocean phenomenon and Reason (2001, 2002) linked SIOD events to austral summer rainfall over coastal eastern South Africa, Mozambique, Zimbabwe and Botswana. SIOD events are also understood to have a major influence over floods and droughts occurring in central and southern Africa, which previously could not be explained by El Nino in the Pacific Ocean or the tropical Indian Ocean Dipole (IOD) mode in the Indian Ocean (Behera & Yamagata, 2001; Reason, 2001; Washington & Preston, 2006).

Moreover, SIOD events have also been shown to significantly influence the different types of southwestern Indian Ocean Tropical Cyclone (TC) trajectories (Ash & Matyas, 2012). However, little work has been done observing the potential influences on Agulhas Current dynamics. SIOD events are only one of the climate phenomena that generate climatic variations in the Southern Hemisphere.

Behera & Yamagata (2001) used EOF analysis to highlight these subtropical dipole SST patterns in the subtropical Indian Ocean (SIO). A positive (negative) phase of the SIOD phenomenon is characterized by positive (negative) SST anomalies in the south-western (north-eastern) region south of Madagascar and negative (positive) SST anomalies in the north-eastern (south-western) off Australia (Behera & Yamagata, 2001). Fauchereau *et al*. (2003) and Hermes & Reason (2004) proceeded to also demonstrate the evolution and forcing of similar dipole SST anomalies in and South Atlantic Ocean (SAO).

Ridderinkhof *et al*. (2010) used moored current observations to show that the IOD phenomenon modulates the wind field anomalies over the tropical Indian Ocean. This modulation would then lead to the adjustment of the South Equatorial Current (SEC). The IOD index was then presented to be closely related to the inter-annual transport variability of the SEC. Through an influence on the SEC, the IOD may also affect the interannual transport variability of the source regions of the Agulhas Current (Stramma & Lutjerharms, 1997).

The hypothesis argued here is that similar to IOD events influencing the SEC through modulations of the wind field anomalies over the tropical Indian Ocean, it then becomes conceivable that SIOD events may in the same way influence the geostrophic velocity at the core of the Agulhas Current, Sea Surface Temperature (SST), and Sea Surface Height (SSH) through similar wind field anomaly modifications in the subtropical Indian Ocean. The motivation for this study is the need for an increased understanding of the SIOD phenomenon and its impact on one of the major currents in the Southern Hemisphere the Agulhas Current, the western boundary current of the Indian Ocean gyre.

.

2. Literature Review

2.1 The Subtropical Indian Ocean Dipole (SIOD)

Atmospheric Global Circulation Models (AGCM) indicate that oceanic and climatic conditions in the Pacific-Indian sector have potential environmental, socio-economic and ecological impacts on the large marine and human populations living in southern Africa (Chiodi & Harrison, 2007), thus it becomes important to understand SIO SST variability.

Model experiments by Reason (2001) demonstrated a near surface low over the warm SST forcing in the south-western Indian Ocean (SW IO) which leads to increased evaporation there, and transport of moist marine airmass towards southeastern Africa where relative convergence and uplift leads to statistically significant increased rainfall.

Behera & Yamagata (2001) additionally put forward that southern African rainfall is also related to positive SIOD events. During positive SIOD events cool SST anomalies are found to be elongated obliquely from the eastern subtropical region to the western tropical region in the southern Indian Ocean (Figure. 1; Upper panel). These cool SST anomalies weaken the maritime ITCZ by suppressing the atmospheric convergence, thus, anomalous south-easterlies spread as far as the equatorial regions of Somalia. This anomalous condition leads to enhanced lower tropospheric south-easterlies which transport the surplus moisture to the far-fetched continental regions in south-central Africa, leading to the moisture convergence there and increased convective activity and anomalous rainfall (Figure. 1; Lower panel). Moreover, increased tropospheric moisture divergence is observed from the eastern subtropical Indian Ocean during the SIOD peak phase. The situation is just opposite during a negative phase.

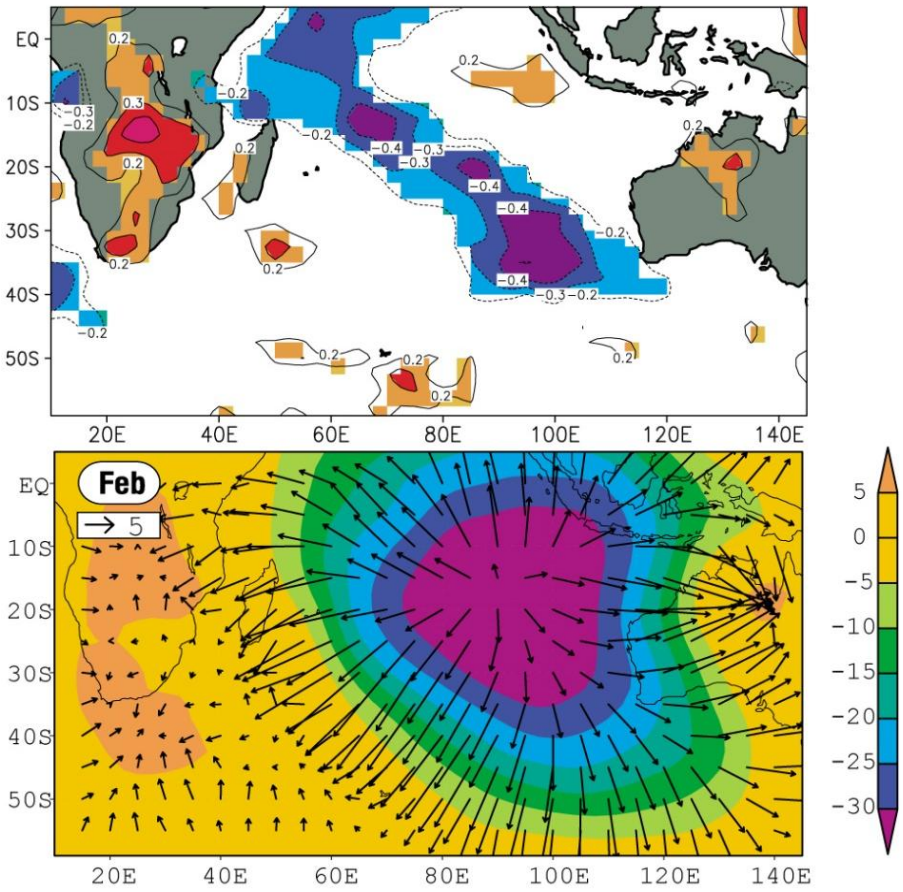

Figure 1: Upper panel; Correlation between rainfall anomalies for the period 1979-98 and the corresponding time series of SDI. Values exceeding 99% of confidence limit (with a two-tailed t test) are shaded. Lower panel; The composite of moisture divergence in February for six SIOD events (see Behera & Yamagata, 2001).

Chiodi & Harrison (2007) argued that positive (negative) SST anomalies tend to occur in the southwestern (eastern) subtropics, in the austral spring to early summer of La Nina years. A reverse pattern is seen to occur during spring/ summer of El Nino years. Albeit, both types of SST anomalies can be seen in years which are neither El Nino nor La Nina (Nicholson, 1997; Reason, 1999; Behera & Yamagata 2001; Chiodi & Harrison, 2007), notwithstanding the fact that even when El Nino and La Nina years are deleted from datasets, the rainfall–SST can still be found (Rocha & Simmonds, 1997; Walker, 1990).

The evolution of anomalous SST during SIOD events has been linked to the strengthening/weakening of the atmospheric subtropical high normally observed in the Sea Level Pressure (SLP) (Behera & Yamagata, 2001). The interannual intensity and movement of the Mascarene High (MH) is important for the SIOD formation (Suzuki *et al*. 2004). The wind on the eastern side of the MH is stronger between 30^0S–20^0S, which is consistent with cooler SST there. The mechanisms for cooling in the eastern pole during a positive mode are strengthened southeasterly trade winds and resultant enhanced ocean surface evaporation and mixing, while the western warm pole develops concurrently with increased poleward Ekman transport of warm waters from tropical latitudes combined with decreased equatorward cold air advection and ocean surface evaporation. During a negative event, the SST anomaly poles are generally reversed, cold air advection and equatorward Ekman pumping occur over the southwestern Indian Ocean in conjunction with more frequent cold frontal passages. Warm air advection is located more frequently over the southeastern part of the basin (Reason, 1999; Venzke *et al*. 2000; Behera & Yamagata, 2001; Qian *et al*. 2002; Hermes & Reason, 2005; Chiodi & Harrison, 2007; Huang & Shukla, 2007b).

Chiodi & Harrison (2007) demonstrated that near-surface humidity, driven by the anomalous meridional advection of water vapour is the main cause of the SST variability in the SIO. The meridional wind anomalies of interest are subsequently found to occur when the subtropical atmospheric anticyclone (MH) is preferentially located toward one of the sides (east) west of the basin.

The ocean mixed layer model used by Chiodi & Harrison (2007) revealed that:

(i) The difference in specific humidity (Δq) anomalies are usually the main cause of this latent heat variability,

(ii) The (Δq) anomalies of interest are driven by the meridional advection of water vapor,

(iii) The formation of the SST anomalies is characterized by abrupt austral summer warming that occurs when moist near-tropical air is advected southward along the western flank of the subtropical anticyclone,

(iv) The position of the subtropical atmospheric anticyclone largely determines the character of these SST anomalies. Modern coupled general circulation model (CGCM) and ocean model studies have determined that the cooling and warming tends to happen simultaneously (Suzuki *et al*. 2004; Hermes & Reason, 2005).

The link between atmospheric variability (i.e., anticyclone modulation) and SST variability has not been precisely determined. Latent heat variability, wind speed, the difference in specific humidity (Δq), and the ocean mixed layer depth have all been implicated in forming and maintaining these SST anomalies (Walker, 1990; Yu & Rienecker, 1999; Behera & Yamagata, 2001; Suzuki *et al*. 2004; Hermes & Reason, 2005; Chiodi & Harrison, 2007).

Suzuki *et al*. (2004) found that these anomalous dipole SST form in late spring to early summer because the ocean mixed layer depth is shallow then, making SST highly sensitive to surface heat flux anomalies. The strongest case has however been made for latent heat flux variability being the main cause of these subtropical SST anomalies in Chiodi & Harrison (2007). Morioka *et al*. (2010) used heat budget analyses of the mixed-layer using outputs from an Ocean General Circulation Model (OGCM) and non-linear statistical analysis called Self Organizing Maps (SOM) for investigating inter-annual SST variations in the southern Indian Ocean. Morioka *et al*. (2010) revealed that shortwave radiation plays a role on mixed-layer depth suggesting that the warming contribution from the increased shortwave radiation becomes even larger because of the reduced mixed-layer depth (MLD).

The cooling tendency by the climatological latent heat flux is enhanced when the mixed-layer depth is reduced despite the fact that the reduced latent heat flux itself introduces the warming tendency (Morioka *et al*. 2010). Subsequently, the MLD undergoes significant variations in the subtropics and any analysis that assumes a constant MLD when investigating the SIOD may have a serious defect (Moison & Niiler, 1998). Hermes & Reason (2005) explain how meridional Ekman heat transport and Ekman upwelling anomalies also contribute to the evolution of the dipole SST anomalies during the SIOD events.

2.2 Subtropical Indian Ocean Dipole Events

Behera & Yamagata (2001) decomposed monthly SST anomalies in the SIO basin using Empirical Orthogonal Function (EOF) and revealed that the leading EOF mode explained about 26% of total variance. Their leading EOF showed values of single polarity dominating the whole analysis domain. They also found a good correlation between the Principal Component (PC) time series of the leading mode and the Southern Oscillation index (SOI). These findings suggest an Indian Ocean warming during the Pacific Ocean El Nino.

The SIOD emerged as the second EOF mode explaining 12% of the total variance, with a northeast-southwest direction. SIOD events are quite robust in the subtropical region of the SIO, however, both the place and the time of occurrences vary slightly among individual events. Typically, SIOD events develop in December-January, peak in February and die down by May-June. Furthermore, during the positive events of 1980-81 and 1981-82 the SIOD did not dissipate completely instead it revived again to become second consecutive event (Behera & Yamagata, 2007).

Morioka *et al*. (2010) indicated that the rainfall anomalies associated with SIOD events are not always the same, such as the 1968 positive SIOD event which, during the austral summer was associated with negative rainfall anomalies in southeastern Africa in contrast to the 1974 and 1981 positive SIOD events which were associated with positive rainfall anomalies over the same region (see list of SIOD events at Table 1).

Negative Dipole Years	Positive Dipole Years
1958	1962
1964	1968
1970	1974
1972	1976
1975	1981
1983	1982
1988	1990
1995	1993
1998	1997
2000	1999
2000	2001
-	2006

Table 1: List of years when positive (negative) dipole events occurred in the South Indian Ocean (Hermes & Reason, 2005).

2.3 The Agulhas Current

This study aims to investigate the influence of SIOD events on the Agulhas Current which is the western boundary current of the Indian Ocean subtropical gyre. With speeds often exceeding 2 ms^{-1} (Bryden *et al*. 2005; Lutjeharms, 2006), the Agulhas Current is the strongest western boundary current in the world's oceans. The Agulhas Current transports, on average, about 70 Sverdrup (where 1 Sv = 106 m^3s^{-1}) of warm, salty water southwards, along the southeastern continental shelf of Africa, from about 27°S to 40°S, where it reverses in a tight retroflection loop to become the Agulhas Return Current (Lutjeharms, 2006; Bryden *et al*. 2005; Rouault & Penven, 2011).

At the retroflection region, large 'Agulhas Rings' are formed carrying warm salty Indian Ocean water, combined with background Agulhas leakage and filaments the rings are shed into the South Atlantic, this exchange of heat and salt forms a vital part of the global thermohaline circulation (Beal *et al*. 2001).

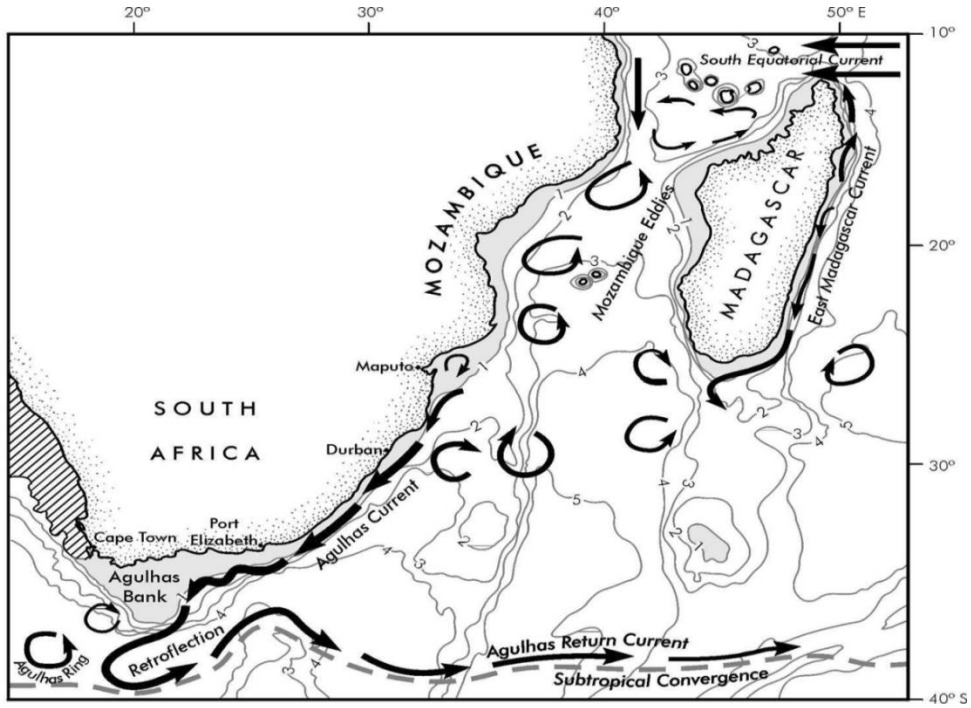

Figure 2: A schematic of the greater Agulhas Current system showing Mozambique Channel Eddies, the East Madagascar Current, the Agulhas Current, the Agulhas Retroflection, and the Agulhas Return Current (Lutjerharms, 2006)

Rouault & Penven (2011) argue that the Agulhas Current is an intense and narrow flow which closely follows the continental shelf from the northern Natal Bight (28°S) to Port Elizabeth (34^0S), moreover, they suggested that the northern Agulhas Current displays remarkably little variability and eddies and plumes constitute the physical oceanography of the southern Agulhas Current, from Port Elizabeth (34°S) to the southern tip of the Agulhas Bank. Grundlingh (1983) & Bryden *et al*. (2005) suggest that the Agulhas Current is in close proximity to the shore for about 80% of the time. Agulhas Current traits are resonant of other western boundary current systems of the world's oceans.

Rouault & Penven (2011) suggest that meanders occur frequently in the Agulhas Current and that these instabilities where first observed by Harris *et al*. (1978) followed by Lutjerharms & Roberts (1988). The latter gave them the name Natal Pulses after their region of origin. Lutjerharms & Roberts (1988) and Bryden *et al*. (2005) showed that Natal Pulses are large solitary meanders in the Agulhas Current associated with a cold water core and a cyclonic circulation inshore of the current.

de Ruijter *et al*. (1999) argued that instabilities in the northern Agulhas Current develop at the Natal Bight, which is an embayment region in the northern Agulhas where the steepness of the continental slope relaxes. However, eddy-resolving simulations by Tsugawa & Hasumi (2010) showed that the Natal Bight is the place where the Mozambique eddy first meets the Agulhas Current and the Natal Bight does not cause the generation of Natal pulses, rather the generation and growth of the Natal pulse occurs because of the interaction between the mean flow of the Agulhas Current and the a Mozambique anticyclonic eddy.

The seasonal cycle of the Agulhas Current has been a point of contention for many years due to scant in situ observations in the region. There are no long-time series of observations to unambiguously define the seasonal cycle of the Agulhas Current therefore studies have been limited to a large extent on model simulations. Despite the Agulhas Current's importance at both global and regional scales, little remains known of the Agulhas Current's variability and there remain ongoing debates around its seasonality. Observational studies in the past were unable to highlight any evidence of a seasonal cycle in the Agulhas Current.

Bryden *et al*. (2005), Matano *et al*. (2008), and Krug & Tournadre (2012) argue that the problem with past analyses of observations in the Agulhas Current is their reliance on Eulerian time-averages of moored observations or the remote sensing variables used to estimate the current's variability. Meinen & Watts (2000) suggest that stream-coordinates are better suited to estimating the true synoptic structure of western boundary currents as they minimize the contamination caused by meandering flows on the time-averaged structure of the current.

Biastoch *et al*. (1999) noted the presence of a seasonal oscillation of the Agulhas Current transport and suggested that its forcing may be wind-driven owing to meridional displacements of the South Indian Ocean anticyclone. Numerical modelling (discussed in Lutjerharms, 2006)

has also demonstrated an annual variation in the transport of the Agulhas Current, for which Lutjerharms (2006) argues that a minimum flow is observed in the austral winter (August) and a maximum flow is observed in austral summer (February). Hermes *et al*. (2007) used an eddy-permitting model to show that the recirculation of the southwest Indian Ocean back into the Agulhas Current is the most significant source region for the volume transport of the Agulhas Current north of 35°S.

Rouault *et al*. (2009) suggested that trade winds are largely responsible for the upstream inertia of the Agulhas Current and an increase in the Agulhas leakage is caused by an increase in the Agulhas Current's total transport. van Seville *et al*. (2009b) argued that a decrease in the upstream inertia leads to an increase in leakage. Beal *et al.* (2011) showed that the Agulhas Current is largely driven by positive wind stress curl over the subtropical Indian Ocean and beyond the southernmost tip of Africa the main controls on retroflection and leakage are the latitude of maximum westerly's and the southward inertia of the Agulhas Current at separation.

Tropical IOD events are now understood to have an influence on the SEC variability through modulations of the wind field anomalies over the tropical Indian Ocean (Ridderinkhof *et al*. 2010). Similarly, it then becomes hypothetically conceivable to assume that SIOD events may in the same way have an influence on the Agulhas Current's dynamic variability and/or SST and SSH mainly though similar mechanisms observed with the tropical IOD – through modifications of the wind field anomaly in the subtropical Indian Ocean.

Until now, there have not been any studies aimed at investigating the influence of SIOD events on Agulhas Current variability after the discovery in 2001 of SIOD phenomena in the SIO (Behera & Yamagata, 2001). In this study, the SIO will be assessed for its dominant modes of variability, with a particular focus on the SIOD. Once the model used in this study has been verified as capable of reproducing the SIOD, a relationship between the SIOD and the Agulhas Current SST and SSH variability will be examined. Furthermore, SIOD phenomena will be statistically examined for an influence on the geostrophic velocity at the core of the Agulhas Current. The main aim is to investigate the means by which positive and/or negative SIOD events influence the dynamic Agulhas Current and Agulhas SST and SSH.

3. Material and Methods

3.1 Model Overview

The Regional Ocean Modelling System (ROMS) is a widely used model with many applications in the southern African region (Penven *et al*. 2006b). ROMS is a split-explicit, free-surface, ocean-only model discretized in coastline and terrain-following curvilinear co-ordinates where higher order numerics and a third-order, upstream-biased advection scheme preserve steep density gradients and reduce dispersion, enhancing precision for a given resolution (Shchepetkin & McWilliams, 2005). ROMS is used solely for oceanic variables and is defined into terrain-following curvilinear co-ordinates can be used to follow coastlines for irregular lateral boundaries which is important for coastal processes.

ROMS is used here as the ARC model configuration (Loveday *et al*, submitted) an eddy permitting implementation of ROMS constructed using ROMSTOOLS (Penven *et al*. 2008). ARC has a resolution of 1/4°, with an Arakawa-C Mercator grid extending from 29°W to 115°E and from 7°N to 48.25°S. Using AGRiF (Debreu & Blayo, 2008), the ARC configuration used here enhances the grid spacing to a twelfth-degree between the region 0° to 40°E and 45°S to 30°S (Loveday *et al*. submitted). The embedded $1/12^0$ (about 2km) "child" nest spans the southern Agulhas Current, Cape Basin, and Southern Benguela. AGIO and ARC are extensions of the SAfE configuration (Southern Africa Experiment, Penven *et al*. 2006; Rouault *et al*. 2009). The vertical resolution of the model is defined by 32 layers which are altered by bathymetry and stretched towards the surface in accordance with Haidvogel and Beckmann's (1999) methods and the thickness of these ranges from the depths to the surface. The ROMS domain (Figure. 3) is shown with the climatological SST map of the SIO with the SIOD boundaries where indices have computed. The blue boxes represent the western subtropical pole (55^0E-65^0E, 37^0S-27^0S) and the eastern subtropical pole (90^0E-100^0E, 28^0S-18^0S) respectively. The green box (25^0E-35^0E, 30^0S-35^0S) represents boundaries of the Agulhas Current region where anomalous SSH and SST anomalies have been assessed for a correlation with the SIOD phenomenon.

Regional bathymetry is derived from the high resolution dataset Global Earth Bathymetric Chart of the Oceans (GEBCO01), http://www.ngdc.noaa.gov/mgg/gebco/gebco.html. To prevent pressure gradient errors, a smoothing of the topography is required. The smoothing is performed so as to maintain the slope parameter (Beckmann & Haidvogel, 1993) everywhere not superior than 0.2. Bottom topography is smoothed towards external bathymetry to limit discontinuity at the boundary. The boundary conditions for this experiment are derived from global ORCA05 model configurations described in Loveday *et al*. (submitted). The model is bulk-forced (Fairall *et al*. 1996) at the surface with the GFDL-CORE v.2b (Large & Yeager, 2004; Large & Yeager, 2009) reanalysis winds and heat fluxes.

In ROMS a suitable numerical algorithm has been implemented to deal with the issues of an optimal combination between time-stepping and mode-splitting: preserving the consistency, accuracy, and stability of the solution. This time-stepping algorithm, functions in such a way that after each time-step of the momentum equations, the derived velocities are without delay used in the calculation of tracer transport and mass balance equations (Shchepetkin & McWilliams, 2005). The numerical schemes for solving time dependent equations are specially designed in such a way that the time-steps of the barotropic (fast) mode are advanced in a series of shorter and faster time-steps, within each baroclinic (large and slow) time-steps. The scheme uses a leap-frog and Adams-Moulton 3-order predictor-corrector, which provides a better numerical stability of the time-steps.

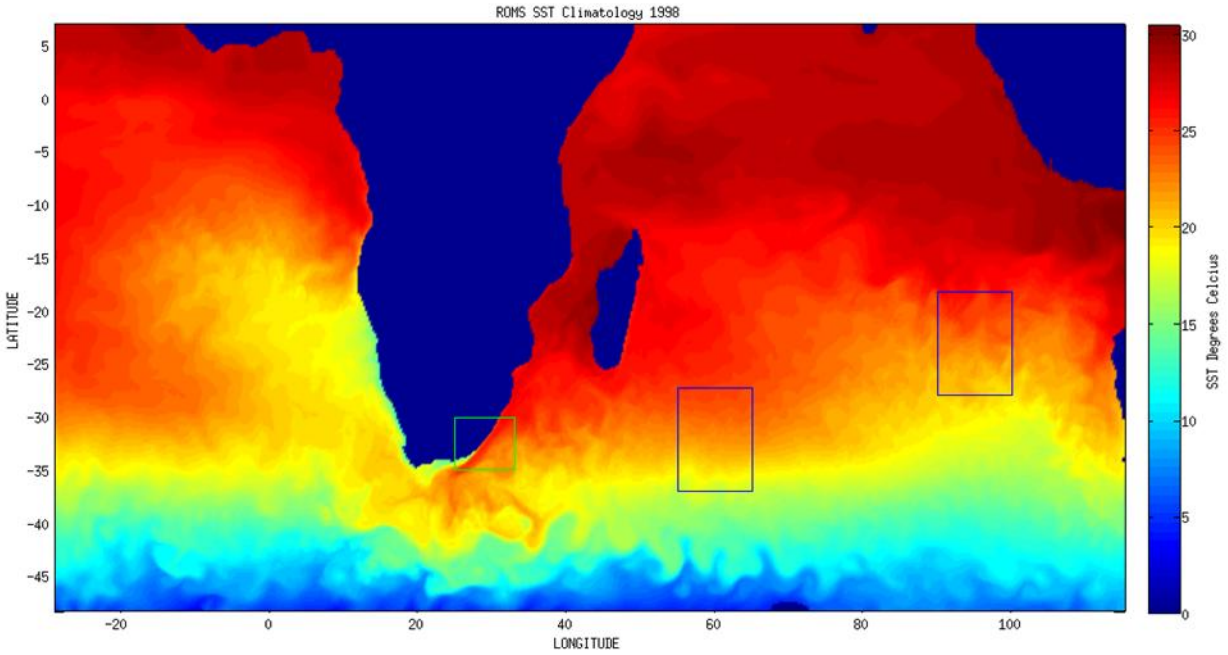

Figure 3: ROMS domain showing SST climatology and poles (blue) where SIOD index has been computed and Agulhas Current region (green) where anomalous SST and SSH has been assessed for a correlation to the SIOD phenomena.

3.2 Empirical Orthogonal Function (EOF)

To explore the SIO as a whole, the linear statistical method EOF analysis (Bretherton *et al*. 1992; Venegas, 1999; Fauchereau *et al*. 2003) was performed in the SIO to evaluate the dominant characteristics of the model SST field such as the dominant space and time patterns. EOF analysis is often used to study possible spatial modes of variability and how they change with time. In statistics, EOF analysis is also known as Principal Component Analysis (PCA) (Bretherton *et al*. 1992). EOF analysis is occasionally classified as a multivariate statistical technique and assumes no priori hypothesis based on some probability distribution hence no statistical test.

EOF analysis is not based on physical principles rather a field is partitioned into mathematically orthogonal (independent) modes which sometimes may be interpreted as atmospheric and oceanographic modes (Venegas, 1999). Typically, the EOFs are found by computing the eigenvalues and eigenvectors of a spatially weighted anomaly covariance matrix of a field. Most commonly, the spatial weights are the cosine (latitude) or, better for EOF analysis, the square root of the cosine of the latitude. The derived eigenvalues provide a measure of the percent variance explained by each mode.

Venegas (1999) describes eigenvalues as not necessarily distinct due to sampling issues and that atmospheric and oceanographic processes are typically 'red' which means that most of the variance (power) is contained within the first few modes. The time series of each mode or Principal Component (PC) is determined by projecting the derived eigenvectors onto the spatially weighted anomalies. This will result in the amplitude of each mode over the period of record.

By construction, the EOF patterns and the principal components are independent. Two factors inhibit physical interpretation of EOFs namely:

(1) The orthogonality constraint and

(2) The derived patterns may be domain dependent (Venegas, 1999). Physical systems are not necessarily orthogonal and if the patterns depend on the region used they may not exist if the domain changes.

Still, even with these short comings, classical EOF (PCA) analysis has proved to be useful (Venegas, 1999). Bretherton *et al*. (1992); Venegas, (1999); and Fauchereau *et al*. (2003) argue that EOF analysis has some tendency to produce spurious spatial patterns especially 'dipolar' structures. In order to assess the robustness of the EOF mode characteristics, two indices are constructed on the basis of the spatial patterns in the second EOF mode by spatially averaging SST anomalies in the southwest subtropical region (55^0E-65^0E, 37^0S-27^0S) and eastern subtropical region (90^0E-100^0E, 28^0S-18^0S) for the period 1958-2000. These regions two regions were chosen primarily because they have been utilized in previous studies (Behera & Yamagata, 2001) and they take into account the strongest SST anomalies even when the domains are extended by 5° North or South. The use of single box averaged indices should avoid the

emergence of artificial anticorrelation structures (Fauchereau *et al*. 2003). The normalized model SIOD index was computed from the SST anomaly difference between the south-western and north-eastern subtropical regions of the SIO.

3.3 Satellite altimetry observations of the Agulhas Current

Snaith & Scharroo (2011) describe a satellite altimeter as a device that uses microwave remote sensing to find a range from the satellite to the surface below it. This is achieved by sending a signal from the satellite and measuring the time delay from when the signal was sent and when a reflected signal is received. This time delay is then corrected for several factors. Radar altimeters are designed to precisely measure wave heights. For a relatively horizontal surface, the nadir point data would have to reach the detector first and after that signals from concentric circles at increasing radius from nadir would be detected within the sensor field of view (Comiso, 2009). For ocean surfaces, the signal is relatively uniform, altered only by different states of the ocean as influenced by wind, ocean current and tides.

Geostrophy dominates the meso and large scale ocean circulation eddies and major current systems are essentially geostrophic, thus with SSH profiles from altimetry we can estimate the geostrophic currents (Robinson, 2004). If SSH can be accurately measured, then an accurate geostrophic current velocity can be calculated. It is this principle that applies satellite altimetry to oceanography. The velocity of the current across track is directly proportional to the slope of the sea surface height along track and the current flow perpendicular to the satellite track along SSH gradients.

Observational data from satellite altimeters was used to characterize the Agulhas Current and its variability along the Topex/Jason altimeter's Track #020, offshore Port Elizabeth (Figure. 4; Krug & Tournadre, 2012). The analysis is based on a stream-coordinate characterization of the Agulhas Current which has allowed better capturing of the intrinsic variability of the Agulhas Current at the annual time-scale. For a more detailed description of the reader is advised to see Krug & Tournadre (2012). The along-track altimetry dataset is obtained from the AVISO

Geophysical Data Records (GDR). The resultant Agulhas Current geostrophic velocity time-series was examined for dominant timescales of variability and correlated to the SIOD index and other climate indices

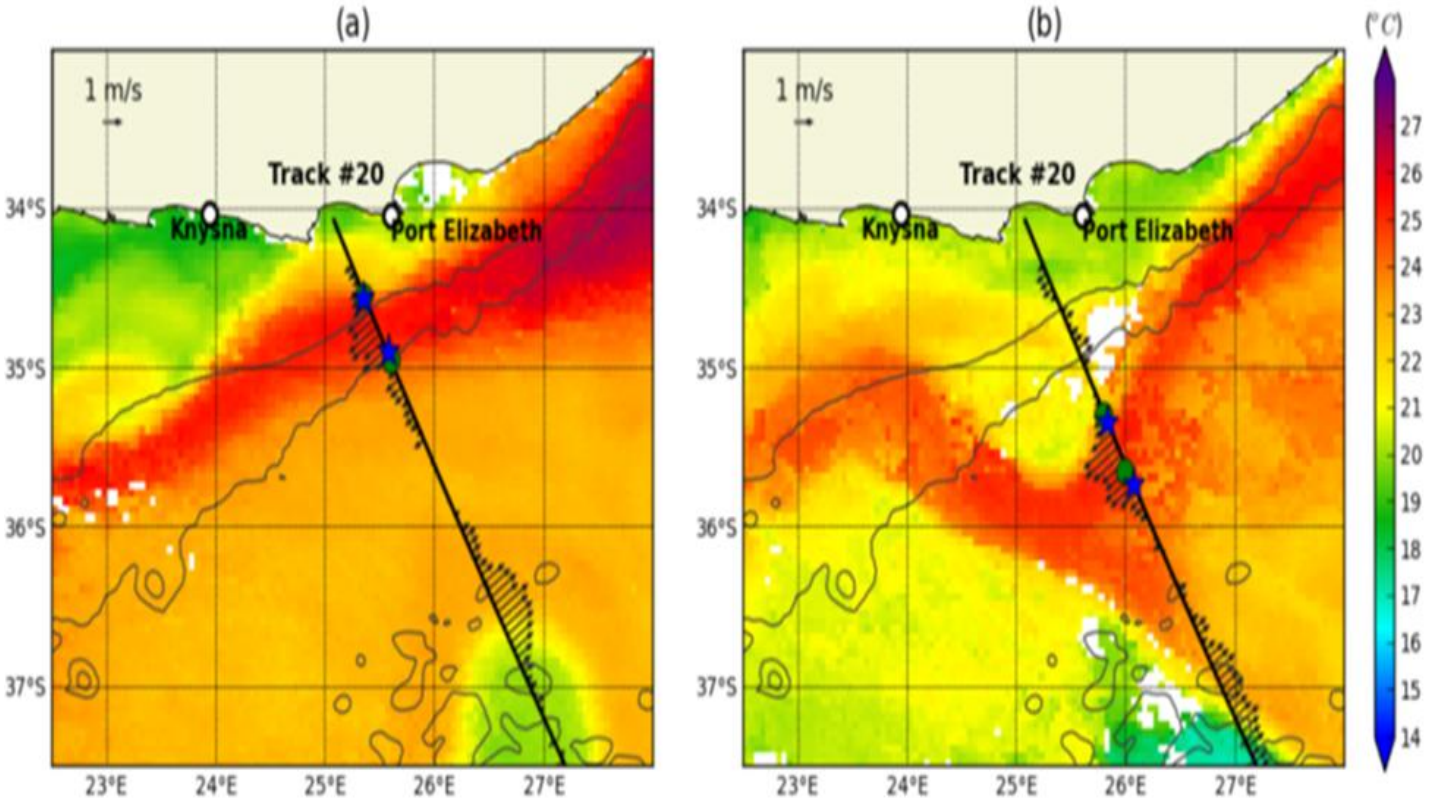

Figure 4: SST maps obtained (a) from 5-day weighted averages centered on the 29th of March 2010 and (b) during the passage of a large offshore meander on the 18th of May 2010. Arrows show the geostrophic currents along Topex-Jason Track #020, offshore Port Elizabeth. The Agulhas Current flow is associated a with local SST maximum and strong south-westerly currents. North-easterly geostrophic currents observed east of 26^0 E marks the position the Agulhas Return Current. Blue stars show the edges of the Agulhas Current's dynamical core estimated by fitting a Gaussian function to the local speed maximum. Green circles show the edges of the Agulhas Current's dynamical core derived from the SST imagery. The 1000m and 3000m isobaths have been plotted as thin black contour lines (taken from Krug & Tournadre, 2012).

3.4 Spectral Analysis

Spectral density (also known as the power density spectrum) estimation is used to estimate the spectrum of a stochastic signal from a time-series sample of a signal in order to characterize the frequency content of the signal (Percival & Walden, 1998). Power Density Spectrum (PDS) is used as a quantitative means to characterize a time series, for instance, they can show how one series differs from another or how two series are related (Percival & Walden, 1998). This technique is used on time series to detect recurrent temporal patterns. In other words, it is a time series analysis method used to isolate the temporal signals blended together inside a single time series (Venegas, 2001). In this study PDS were used on model output and the observational data.

3.5 Wavelet Analysis

Wavelet transforms have been used in various studies to investigate the temporal variability in time series derived from the observational and model data (Torrence & Compo, 2005). Wavelet analysis attempts to solve these problems by decomposing a time-series into time/frequency space simultaneously. Wavelets can also show the evolution in the relative strength of the dominant modes with time through a time-series, hence it has been used in this study. Wavelets have also been successfully used in other oceanic applications such as the investigation of equatorially trapped waves (Meyers *et al*. 1993), the study of intra-seasonal variability in surface winds over the Benguela upwelling system (Risien *et al*. 2004), and investigating the source regions of the Agulhas (Hermes & Reason, 2007) to name a few.

3.6 Observational SIOD Index

The observed SIOD index is taken from the Hadley Centre Sea Ice and Sea Surface Temperature data set (HadISST1) which is satellite data on a one degree latitude-longitude grid for the period 1958-2007 except for 2007 April onwards, that was derived from the National Oceanic and Atmospheric Administration's (NOAA) Optimum Interpolation (OI) Sea Surface Temperature (SST) (Behera & Yamagata, 2001). The observed and model normalized SIOD index was computed from the SST anomaly difference between the south-western (55^0E-65^0E, 37^0S-27^0S) and north-eastern (90^0E-100^0E, 28^0S-18^0S) subtropical regions of the SIO. The model simulated SST anomalies were also compared to the observational SST anomalies from Behera & Yamagata (2001).

3.7 The ENSO Index

The ENSO index (Rayner *et al*. 2003) used in this study is a monthly ERSST.V3B Niño index product. It is the most recent version of the Extended Reconstructed Sea Surface Temperature (ERSST) analysis is v3b. The analysis is based on the International Comprehensive Ocean-Atmosphere Data Set (ICOADS) release 2.4. At the end of every month, the ERSST analysis is updated with the available GTS ship and buoy data for that month. The anomalies are computed with respect to the 1971-2007 monthly climatology (Xue *et al*. 2003)

3.8 The IOD Index

The IOD index used in this study was sourced from the webpage link http://www.jamstec.go.jp/frcgc/research/d1/iod/DATA/dmi_HadISST.txt. This product is the Met Office Hadley Centre's sea ice and sea surface temperature (SST) data set, HadISST1.

It replaces the Global Sea Ice and Sea Surface Temperature (GISST) data sets, and is a unique combination of monthly globally-complete fields of SST and Sea Ice concentration on a 1^0 latitude-longitude grid from 1870 to date (Rayner *et al*. 2003).

3.9 NCEP-NCAR reanalysis

NCEP/NCAR reanalysis data used is from the Twentieth Century Reanalysis Project, which is supported by the Earth System Research Laboratory Physical Sciences Division from the NOAA and the University of Colorado CIRES/Climate Diagnostics Centre. The Twentieth Century Reanalysis Project is an effort to produce a global reanalysis dataset spanning the entire twentieth century, assimilating only surface observations of synoptic pressure, monthly sea surface temperature and sea ice distribution. Products include 6-hourly ensemble mean and spread analysis fields on a 2x2 degree global latitude/longitude grid, and 3 and 6-hourly ensemble mean and spread forecast fields on a global Gaussian T-62 grid. Fields are accessible in yearly time series files (1 file/parameter) or monthly synoptic files (Compo *et al*. 2008).

3.10 Modern Era-Retrospective Analysis for Research and Applications

The Modern Era-Retrospective Analysis for Research and Applications (MERRA) supports NASA's Earth science objectives, by applying the state-of-the-art GEOS-5 data assimilation system that includes many modern observing systems such as EOS in a climate framework. The MERRA time period covers the modern era of remotely sensed data, from 1979 through the present, and the special focus of the atmospheric assimilation is the hydrological cycle. Previous long-term re-analyses of the Earth's climate had high levels of uncertainty in precipitation and inter-annual variability.

3.11 Composite Map Analysis

Composite map analysis is a technique used by climatologists to identify consistent spatial patterns in relationships (Flower, 2005). Here, austral summer (JFM) average Agulhas Current SST and SSH composite maps were used to highlight the main features of the SIOD events, by reducing the noise of individual cases. SIOD events were chosen by visual examination of the model simulation output. When applied to gridded SST/SSH model data, composite analysis involved observing for patterns within the fields, typically expressed in terms of anomalies relative to a time period of interest. These composite maps were then interpreted in terms of associated impacts on the Agulhas Current SST and SSH intensity and/or strength which in turn may be verified by statistical relationships. The primary purpose of composite mapping here was to investigate whether there are consistent patterns in Agulhas Current SST/SSH anomaly fields associated with potential forcing factors or some consequent impact, in this case the SIOD events of the subtropical Indian Ocean.

3.12 Research Questions

The key questions examined by this study include firstly, an investigation of whether the ARC configuration (Loveday *et al*. submitted) of ROMS with a particular resolution increase around South Africa is capable of producing SIOD phenomena with characteristics comparable to those of observational SIOD datasets.

Secondly, questions regarding model SIOD phenomena time-scales of variability will be examined compared and contrasted to those of the observed SIOD datasets. This is done to examine whether SIOD SST periodicities affect the Agulhas Current's variability and if so to what extent. Furthermore, a statistical correlation will be investigated between Agulhas Current variability and SIOD phenomena.

Ultimately, the connection between SIOD phenomena and the satellite derived geostrophic velocity at the core of the Agulhas Current will be explored. This is done to ascertain whether SIOD phenomena are the forcings behind the annual cycle in the geostrophic velocity observed

in the Agulhas Current by Krug & Tournadre (2012). Furthermore, questions regarding how positive and/or negative SIOD composites influence anomalous SST and/or SSH in the Agulhas Current region will also be explored.

4. Results

4.1 Introduction

As discussed seen earlier the SIOD has been established to have an important impact on coastal eastern South Africa, Mozambique, Zimbabwe and Botswana summer rainfall patterns (Behera & Yamagata, 2001; Reason, 2001, 2002). This section will describe the ability of the ROMS configuration to accurately simulate the SIOD phenomena. Furthermore, this section will describe how the anomalous model SIOD events influence (*i*) the anomalous satellite derived geostrophic velocity at the core of the Agulhas Current and (*ii*) Agulhas Current SST and SSH during SIOD events. EOF Analysis, Wavelet Analysis and Composite Analysis were used investigate SIO SST variability.

Similar to the tropical IOD, (Ridderinkhof *et al*. 2010) the assumption made by this study is that SIOD events modulate large scale winds over the SIO leading to cyclonic (anticyclonic) during negative (positive) events. It is then based on this hypothesis that this study attempts to show that SIOD phenomena contribute to the inter-annual variability of the Agulhas Currents. Here SIOD events are defined as those events when absolute Subtropical Diploe Index (SDI) value exceeds one standard deviation. Positive (Negative) SST anomalies exceeding one standard deviation imply a SIOD event, however an assessment of the time-series alone is not enough to confirm SIOD events therefor other methods where applied in order to examine the SIO SST and SSH variability further. The methods used to unambiguously define SIOD events will be discussed later in the chapter.

4.2 Model Validation & Climatology

The model was validated using data from the 2009 World Ocean Atlas (WOA) product which is a set of objectively analyzed 1° grid climatological fields of *in situ* temperature, salinity, dissolved oxygen etc. During comparisons between model and WOA SST fields the model SST was observed to exhibit a warm temperature bias near the equator, however both SST fields displayed a strong temperature gradient (Suzuki *et al*. 2004) in the subtropical regions south of 30°S (Figures. 5 & 6).

The model 28° isotherm (Manganello, 2007) which is generally used as a proxy for the geographical extent of the warm pool and its location exhibits a SW-NE orientation with warmer water to the west of the Indian Ocean basin between 30°S - 20°S during the austral summer (Suzuki *et al.* 2004) in the model and WOA SST product. The model tends to overestimate the spatial spreading of the 28^0 isotherm nevertheless. The SW-NE orientation reverses during austral winter. A meridional SST gradient of roughly 0.0025°C per km in WOA09 and 0.0027°C per km in ROMS can be observed in the 12 month climatology's from the equatorial region to 45°S in the SIO for the period 1958-2007. Furthermore, the Agulhas Current in the model can be identified by the steep SST gradient of about 10°C $(100km)^{-1}$ according to Rouault *et al*. 2002 offshore the east coast of South Africa between the current and surrounding ocean. The Agulhas Current appears to be well resolved (Figures. 5 & 6). The reader is referred to Loveday *et al.* (submitted) for a comprehensive account of validation of the model in the Agulhas Current region.

The annual cycle of the ITCZ varies significantly both in location and migration between West Africa and the Atlantic on one hand, and East Africa and the Indian Ocean on the other hand. The ITCZ migrates north and south reaching its southern most position during the austral summer at approximately 9^0S. Impacts from the monsoon on circulation play active roles in the SEC's velocity and direction and this may affect the total transport downstream at the Agulhas Current through the flow east of Madagascar and Mozambique Channel eddies. Modern studies have not yet established the monsoon's influence on the Agulhas Current.

During austral summer, warm zonally stretched SST isotherms are found across the central and northern Indian Ocean with a meridional displacement from the equator to approximately 45° S both in the model and observed data (Figures 5 & 6). During austral winter the ITCZ moves to approximately 9^0N and SST in the central and NE regions of the IO cools dramatically.

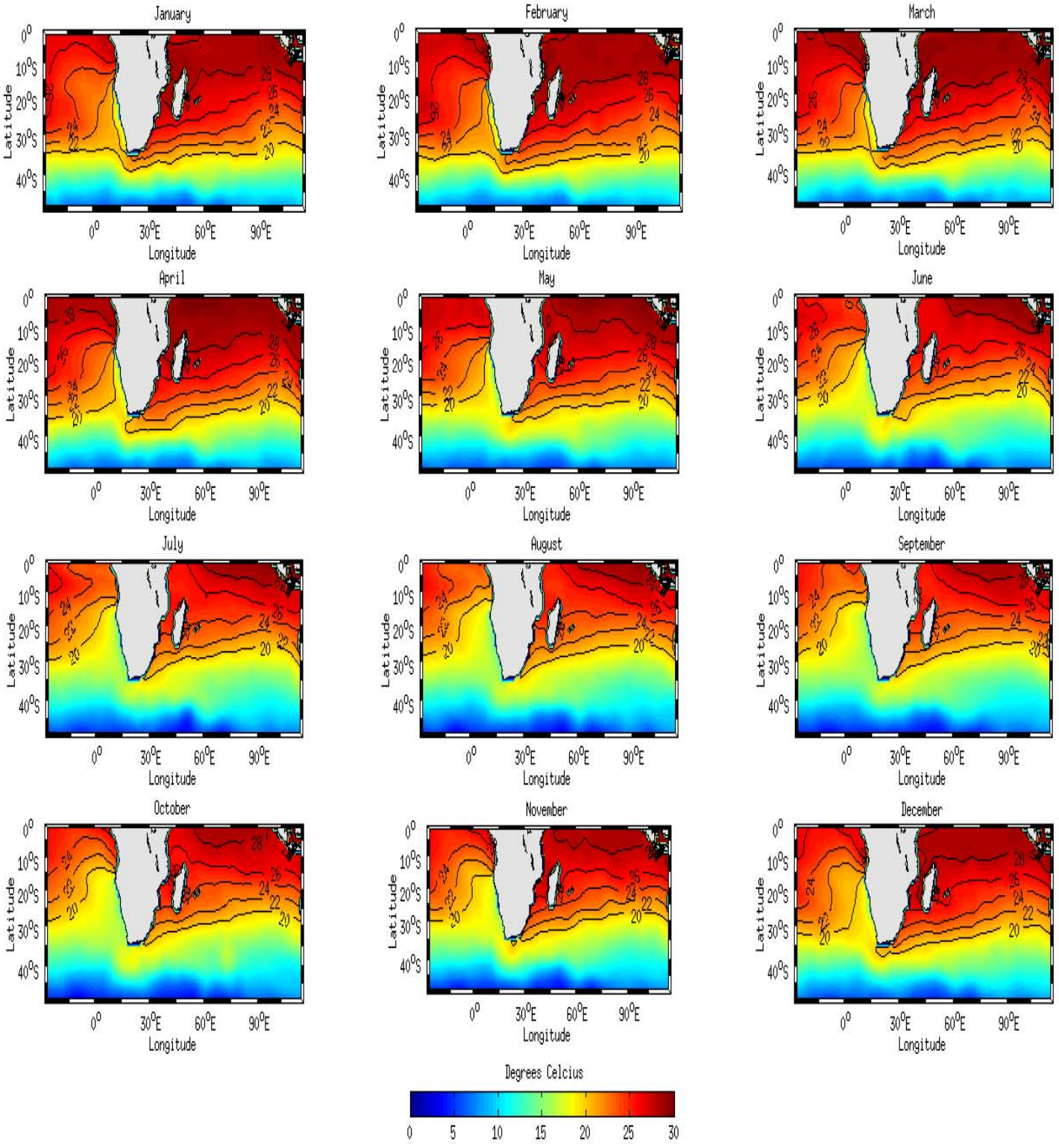

Figure 5: World Ocean Atlas (2009) monthly SST climatological mean in the Indian Ocean based on the period 1958-2007 showing the 28^0 isotherm.

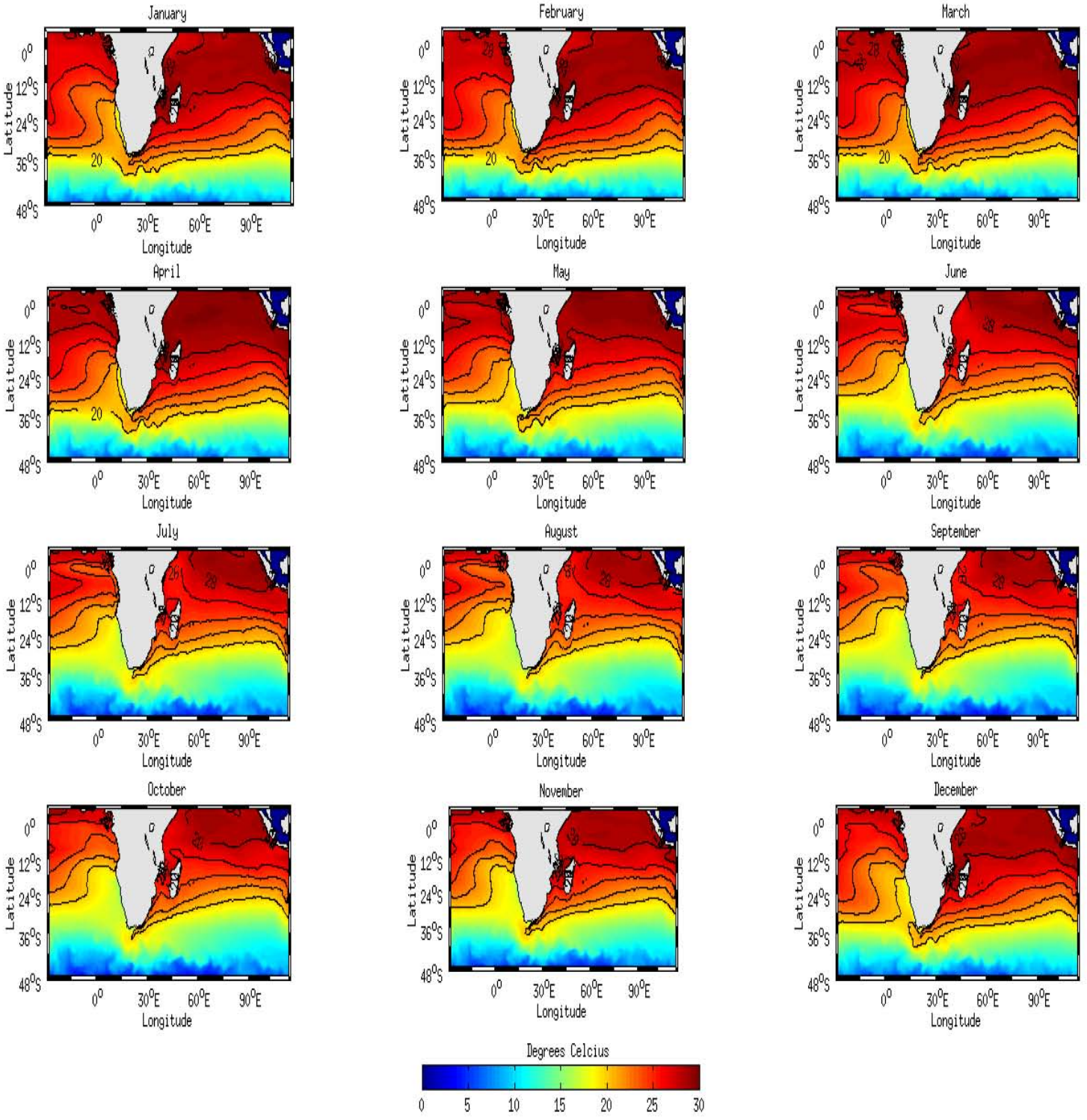

Figure 6: ROMS monthly SST climatological mean in the Indian Ocean based on the period 1958-2007 also showing 28^0 isotherm.

4.3 NE and SW IO anomaly patterns

The time series of normalized the monthly SST anomalies found in the NE and SW IO SST poles of the SIO is shown in figure 7. The figure allows for a clear observation of the times when the two poles are in or out of phase with each other by display SIOD patterns alongside each other. Large positive (negative) anomalies in the SW and large negative (positive) anomalies in the NE IO imply positive (negative) dipole events. The amplitude of the anomalies determines the strength and phase of the SIOD event. Nevertheless, an assessment of the time-series alone is not sufficient to confirm SIOD events and their spatial characteristics therefore other methods will be explored in order to investigate the SIO SST and SSH variability.

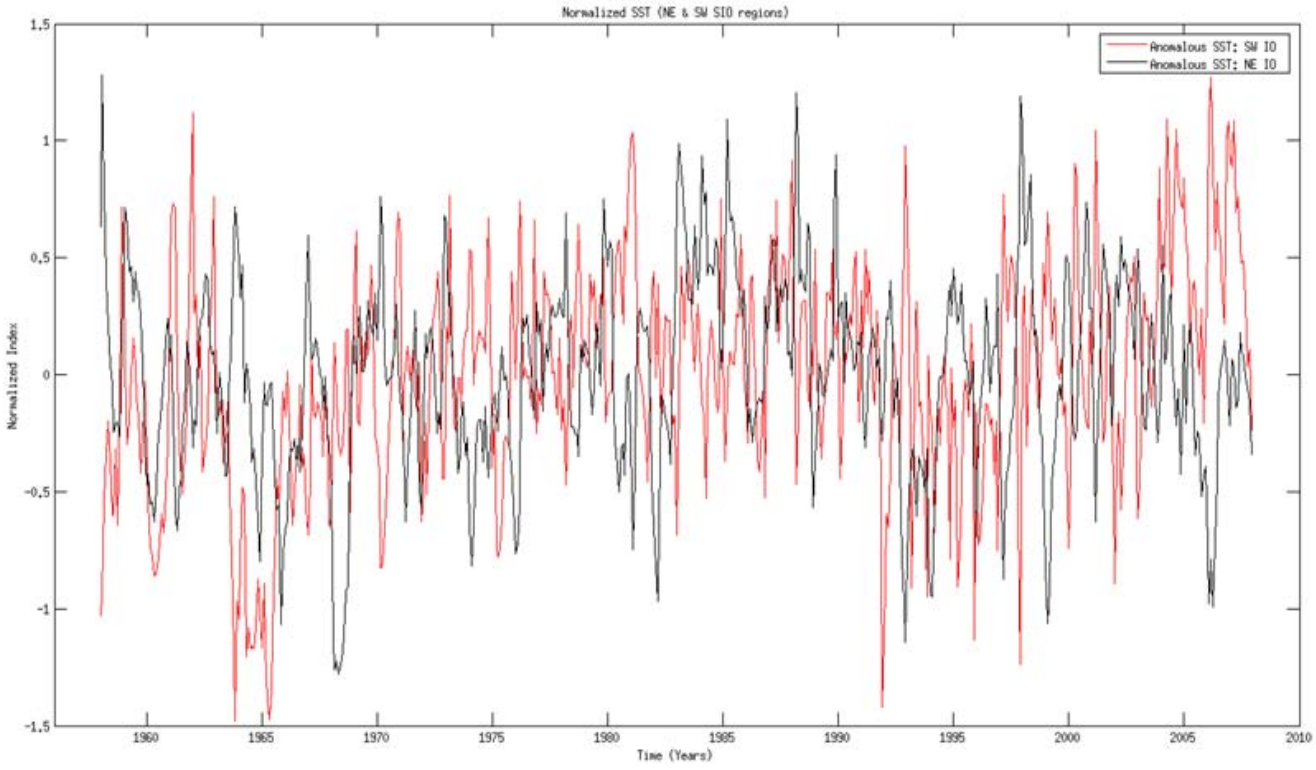

Figure 7: ROMS SST anomalies for the eastern subtropical pole (55^0E-65^0E, 37^0S-27^0S) and western subtropical pole (90^0E-100^0E, 28^0S-18^0S) of the subtropical Indian Ocean basin for the period 1958-2007.

4.4 SST variability in the NE IO

The previous section presented how the model SST compares with the WOA09 SST product, this section will see the continuous use of the model to explore temporal variability of the SST in the SIO using wavelet analysis and EOF. The time series have been normalized wherever wavelet analysis has been performed.

In the model wavelet analysis results suggest that the NE IO region's (off Australia) SST variability displays periodicities in both the high and low frequency parts of the wavelet spectrum. In the high frequency, NE IO SST demonstrates periodicity in the order of 5-12 and 15-24 months significant particularly during mainly during the years 1965-1975 and 1995-2000 respectively (Figure. 8b, c). Low frequency inter-annual variability in the model was observed in the order of 78 months significant particularly during the years 1970-1985.

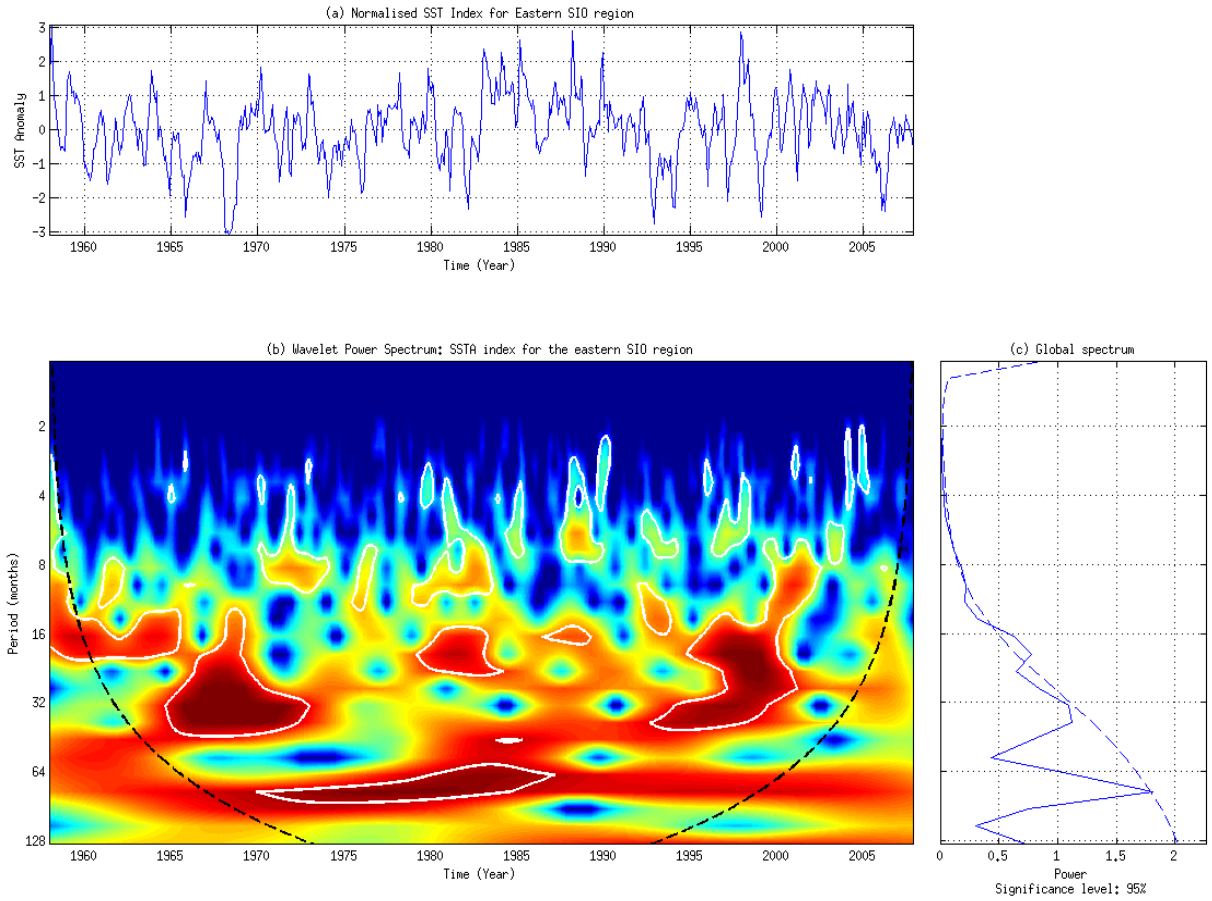

Figure 8: (a) The normalized time-series of the ROMS SST variability for the NE IO (90^0E-100^0E, 28^0S-18^0S), (b) wavelet spectrum for the period 1958-2007, alongside (c) the global power spectrum. The white contours represent the 95% significance regions. The cone-of-influence is represented by the dotted black line and it represents the region of the wavelet spectrum where the edge effects become important. In cases where the end-points are unimportant, the COI can be disregarded (Meyers *et al*. 1993).

4.5 SST variability in the SW IO

The SW IO (south of Madagascar) region's SST variability demonstrates greater variability in comparison to the NE IO, interestingly all of this region's significant variability is found in the high frequency. SST variability in the SW IO is shown by wavelet analysis to have a high frequency semi-annual to annual periodicity in the order of 4-15 months variability. This high frequency periodicity was significant particularly during the years 1960-1965 and 1993-1995

(Figure. 9). After examining and assessing the two defined regions of the SIO a broad understanding of the characteristics of the larger SIO domain need to be investigated in order to get a clearer understanding of what drives the smaller scale SST dynamics.

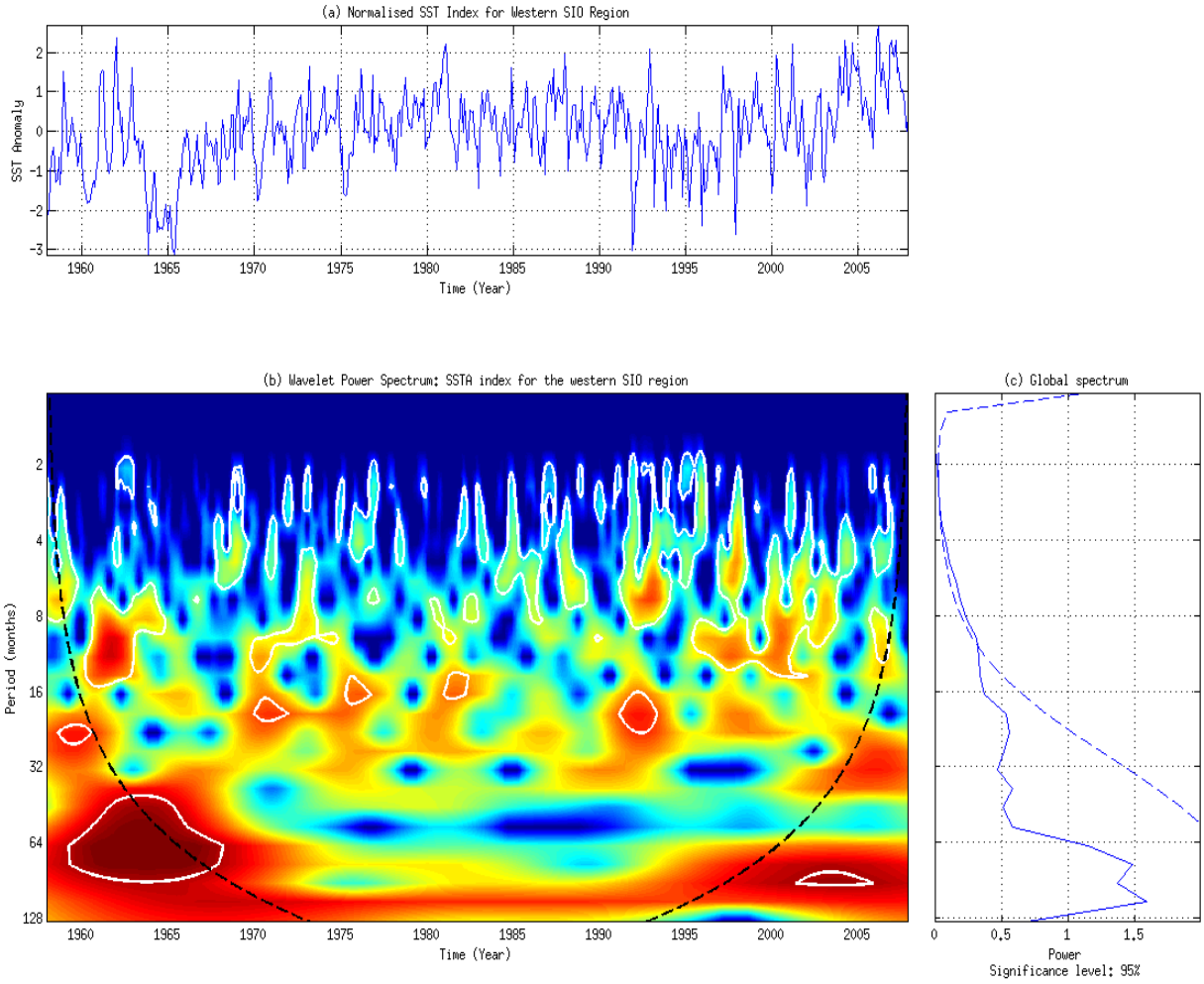

Figure 9: Same as Figure 8 but for the western Indian Ocean region (55^0E-65^0E, 37^0S-37^0S).

4.6 EOF Analysis of the subtropical Indian Ocean

In the previous section, wavelet analysis has revealed semi-annual to annual and inter-annual cycles in the SST variability of the NE and SW IO regions. To explore the SIO as a whole, EOF analysis was then performed in the model SST to investigate the dominant modes of variability in the SIO basin from monthly anomalies of the period 1958-2007 in the region (10^0S-45^0S, 40^0E-114^0E) of the SIO.

The purpose of EOF is to identify dominant modes of variability as each mode is a combination of a spatial pattern and a time series, and represents a certain fraction of the total variance. When applied to monthly SST anomalies the leading EOF mode explained about 13.66% of the total variance and shows values of single polarity dominating the analysis domain (Figure. 10a, d). The interesting SIOD pattern emerged oriented in the northeast-southwest direction as the second EOF mode explaining 8.93% of the total variance in the model SIO (Figure 10b, e). The third EOF mode exhibited a monopole spatial pattern with and explained only 6.39% total variance in the model SIO (Figure 10c, f).

The model PC2 component of the second EOF (Figure 10e) is very similar to the model anomalous SIOD and the observed SIOD index defined by Behera & Yamagata (2001). There are slight differences however in the amplitudes and timing of the model SIOD, observed SIOD and model PC2 component indices.

The SIOD has been identified as showing the strongest signal during austral summer months (Behera & Yamagata, 2001; Fauchereau *et al*. 2003; Hermes & Reason, 2005, Chiodi & Harrison, 2007; Morioka *et al*. 2012). Suzuki *et al.* (2004) related the SIOD to austral summer/autumn, primarily because the depth of the surface MLD is shallowest at that time. This enhances (suppresses) warming of the mixed layer by climatological shortwave radiation, leading to the generation of the positive (negative) SST anomaly pole Morioka *et al*. (2012). Chiodi & Harrison (2007) argued that wind-driven latent heat flux anomalies are the major factor in the anomalous SST evolution and they influence the SST most efficiently during the austral summer. It is these arguments and findings by Behera & Yamagata (2001) that have motivated

for another EOF analysis to be performed for only the austral summer months (Figure. 11) which have been defined in this study as being January, February, and March (JFM).

An examination into austral summer SIO SST variability yielded the SIOD to emerging as first mode of variability in the domain with a 20.84% explained variance (Figure. 11a, d). The second EOF mode explained 14.13% and third EOF mode explained 9.12% of the total JFM variance in the model SIO (Figure. 11b, c, d, e, and f) from 19°8-2007.

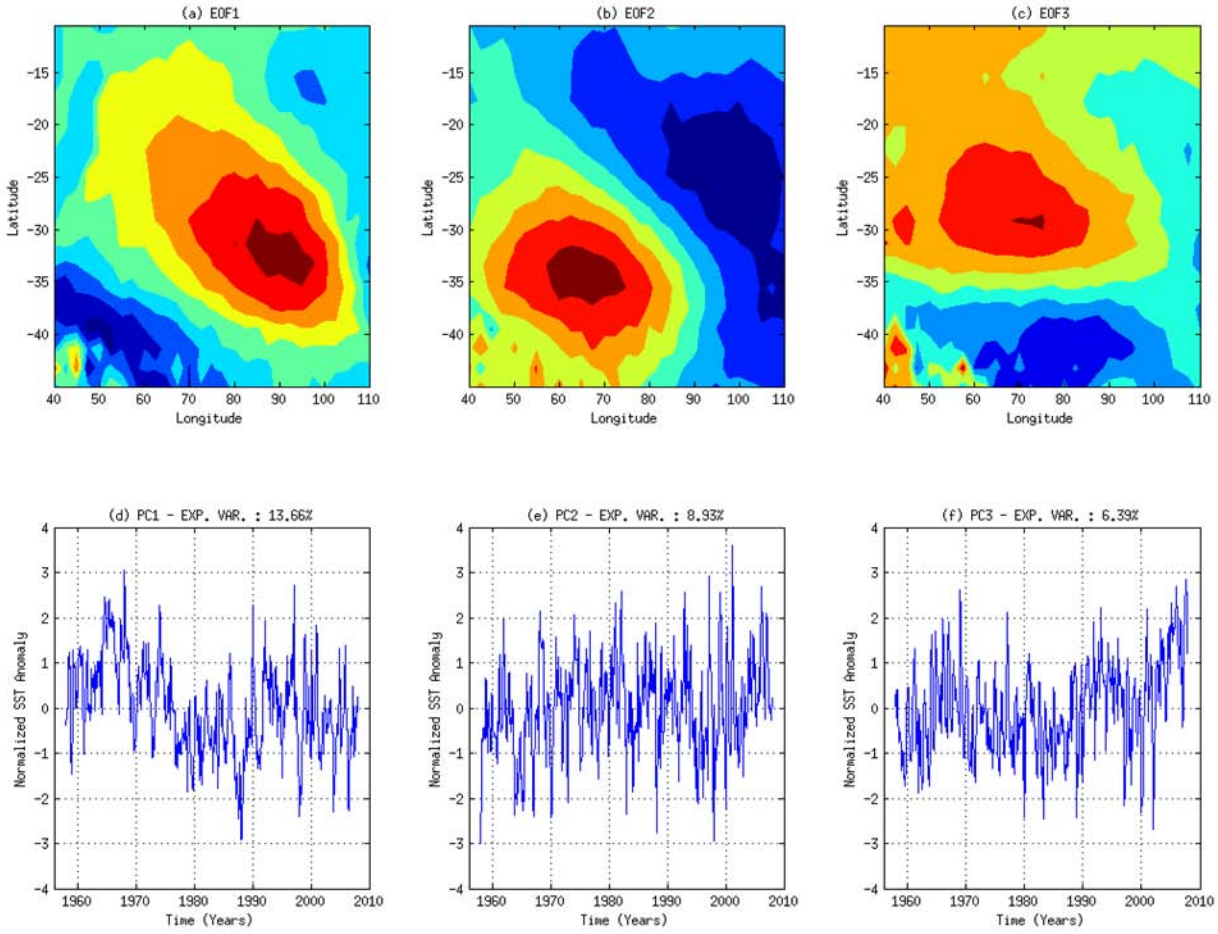

Figure 10: EOF analysis applied on ROMS monthly SST anomalies for all the months in all the years. EOF spatial patterns (a, b and c) and time series (d, e and f) for the EOF modes of variability for the period 19°8 to 2007 in the subtropical Indian Ocean (10^0S-45^0S, 40^0E-110^0E).

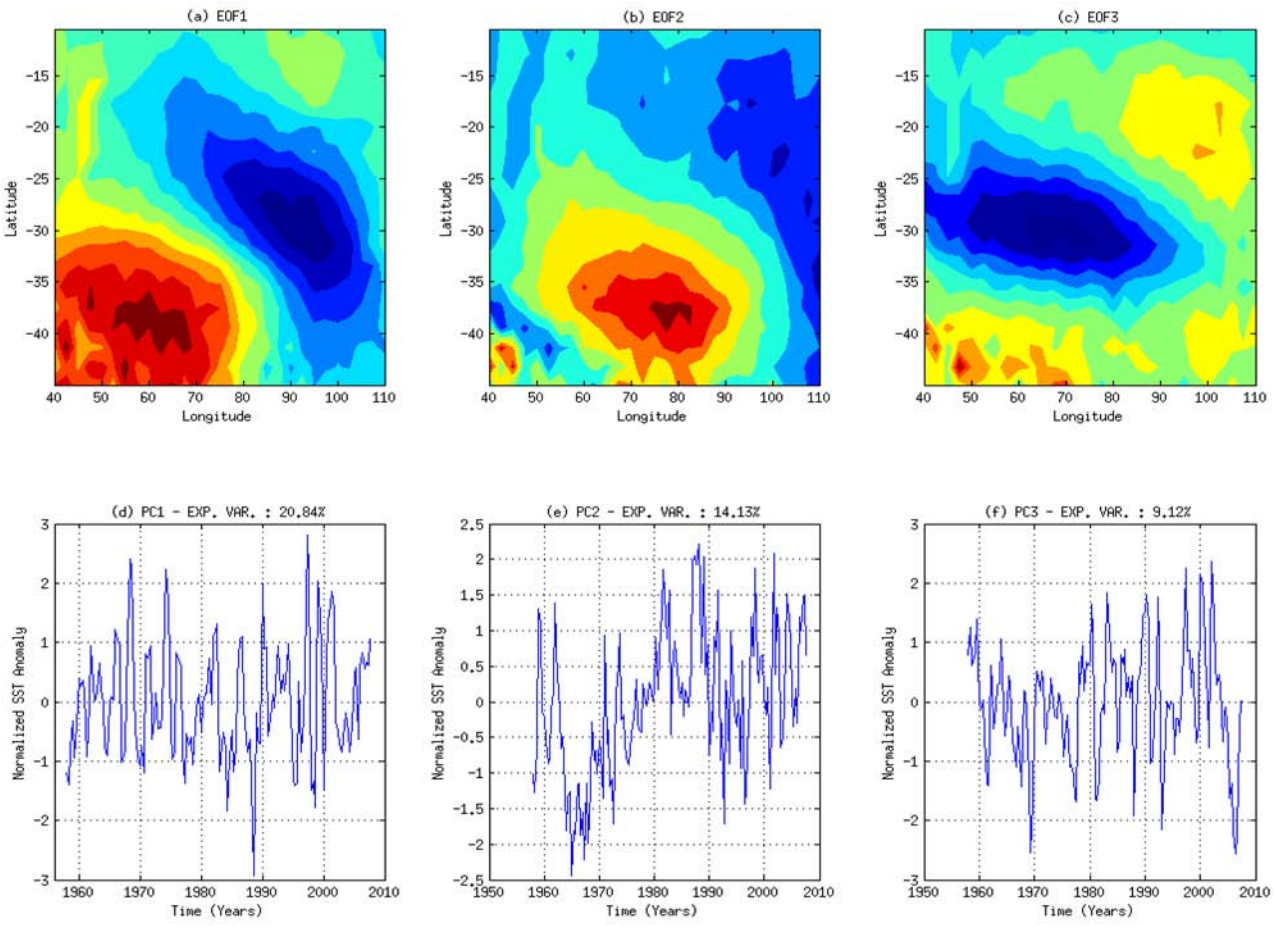

Figure 11: EOF analysis applied on ROMS monthly SST anomalies for only the austral summer (JFM) months. EOF spatial pattern (a, b and c) and time series (d, e and f) for the EOF modes of variability for the period 1958 to 2007 in the subtropical Indian Ocean (10^0S-45^0S, 40^0E-110^0E).

4.7 EOF PC2 component and ROMS SIOD Index wavelet analysis

The EOF analysis applied on the model SST for all the months from January through to December for all the years since 1958 to 2007 yielded the SIOD as the second mode of variability in the SIO, moreover, it is this section that will present an examination of the spatial and temporal characteristics of the EOF PC2 component and ROMS SIOD Index through wavelet in order to ascertain periodic frequency cycles. Thus far the study has been able to describe the SIOD from the model SST using anomalous NE and SW IO SST and EOF analysis.

The SDI was computed from a SST anomaly difference between the SW and the NE poles of the SIO (Figure. 3). By creating this SIOD index it became possible to identify true dipole years from spurious ones. True SIOD events occurred in those years when the absolute SDI value exceeded one standard deviation and the dipole pattern had to be oriented in a northeast-southwest direction, furthermore, the polarity between the two anomaly poles should be undoubtedly clear. On the basis of these classifications, identified SIOD events through the SDI were verified by visual examination of the anomalous ROMS SST dataset and compared to EOF analysis results. Events which did not fully satisfy these conditions were excluded.

The anomalous model SIOD index was then correlated to the anomalous observed SIOD index, in which the results showed a high correlation (r = 0.83 at 95% confidence interval). This suggests great consistency between the ROMS SST and observational SST data in the SIO domain (Figure 14). The EOF PC2 component and ROMS SIOD index also have a high correlation value (r = 0.91 at 95% confidence interval). This simply means that the EOF analysis is highly skillful at reproducing SIOD phenomena in the model. This suggest that the model can be trusted to faithfully reproduce SIOD SST trends, notwithstanding the fact that model solutions have discrepancies hence there are some inconsistencies between the model index and the observation index and the correlation is not perfect. This may be caused by errors in the fluxes or model physics. Despite all the possible sources of error, the correlation coefficient between the model and observations remains very high.

EOF PC2 component wavelet analysis results suggest a high frequency annual cycle in the PC2 component in the order of 8 – 12 months particularly between the years 1995-2000 for the period 1958-2007 (Figure. 12b, c). Low frequency inter-annual variability was observed in the order of 78 months, significant particularly from 1975-1990 (Figure. 12b, c).

Similarly, wavelet analysis performed on the anomalous model SIOD index suggests comparable results obtained from the EOF PC2 component (Figure. 13). At high frequency the model SIOD index suggests a semi-annual to annual cycle in the SDI index in the order of 4 – 13 months significant particularly during the years 1960-1965, 1980-1985 and 1990-2000. Another periodic high frequency signal is observed at 20 - 24 months mainly in 1980-1985 and 1990-2000. Inter-annual variability is observed in the low frequency at 78 months. This low frequency signal is

not consistent throughout the period of 1957-2007 it showed significant periodicity during the years 1970-1975 and 1998 (Figure. 13).

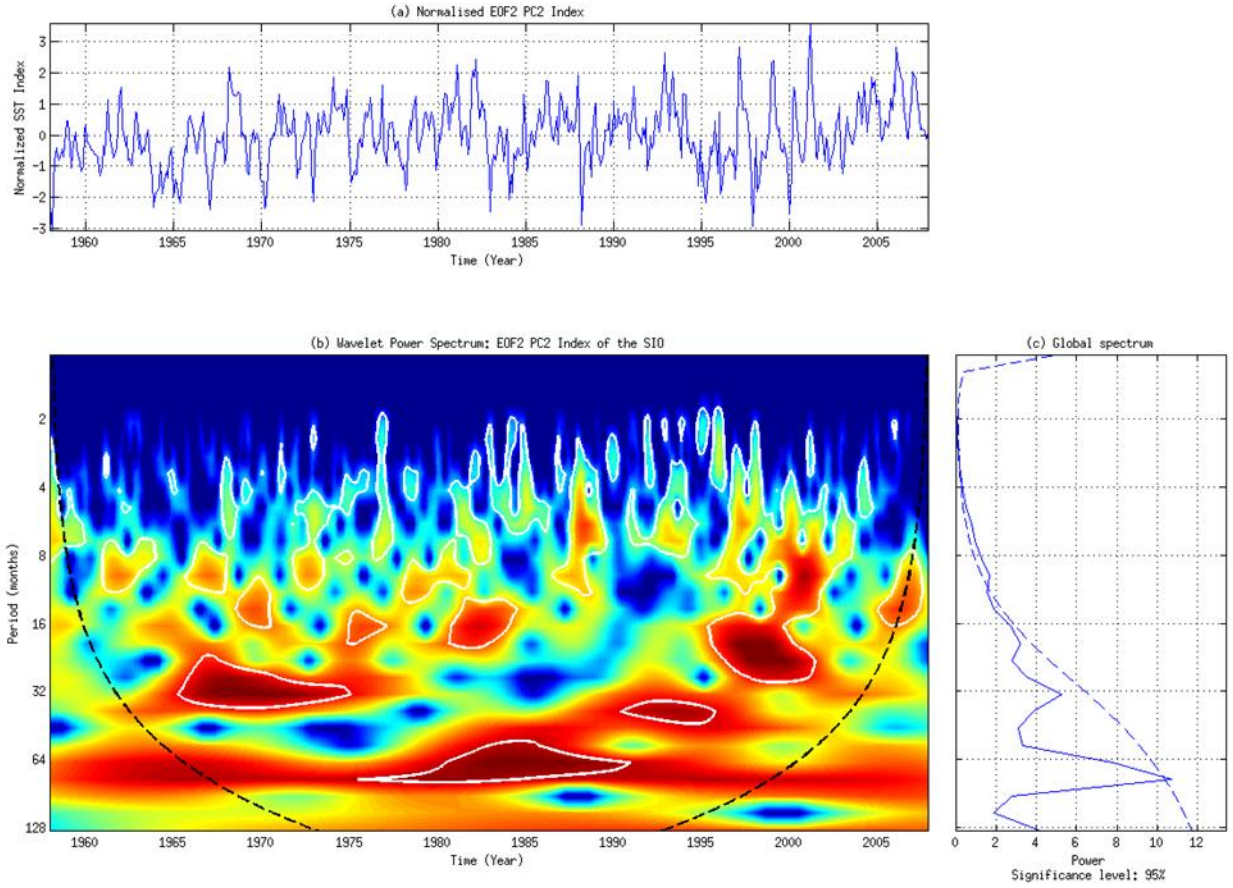

Figure 12: (a) Wavelet analysis applied on the ROMS monthly (all months) PC2 component of the 2nd EOF mode of the subtropical Indian Ocean (10^0S-45^0S, 40^0E-110^0E), (b) wavelet spectrum for the period 1958-2007, alongside (c) the global power spectrum.

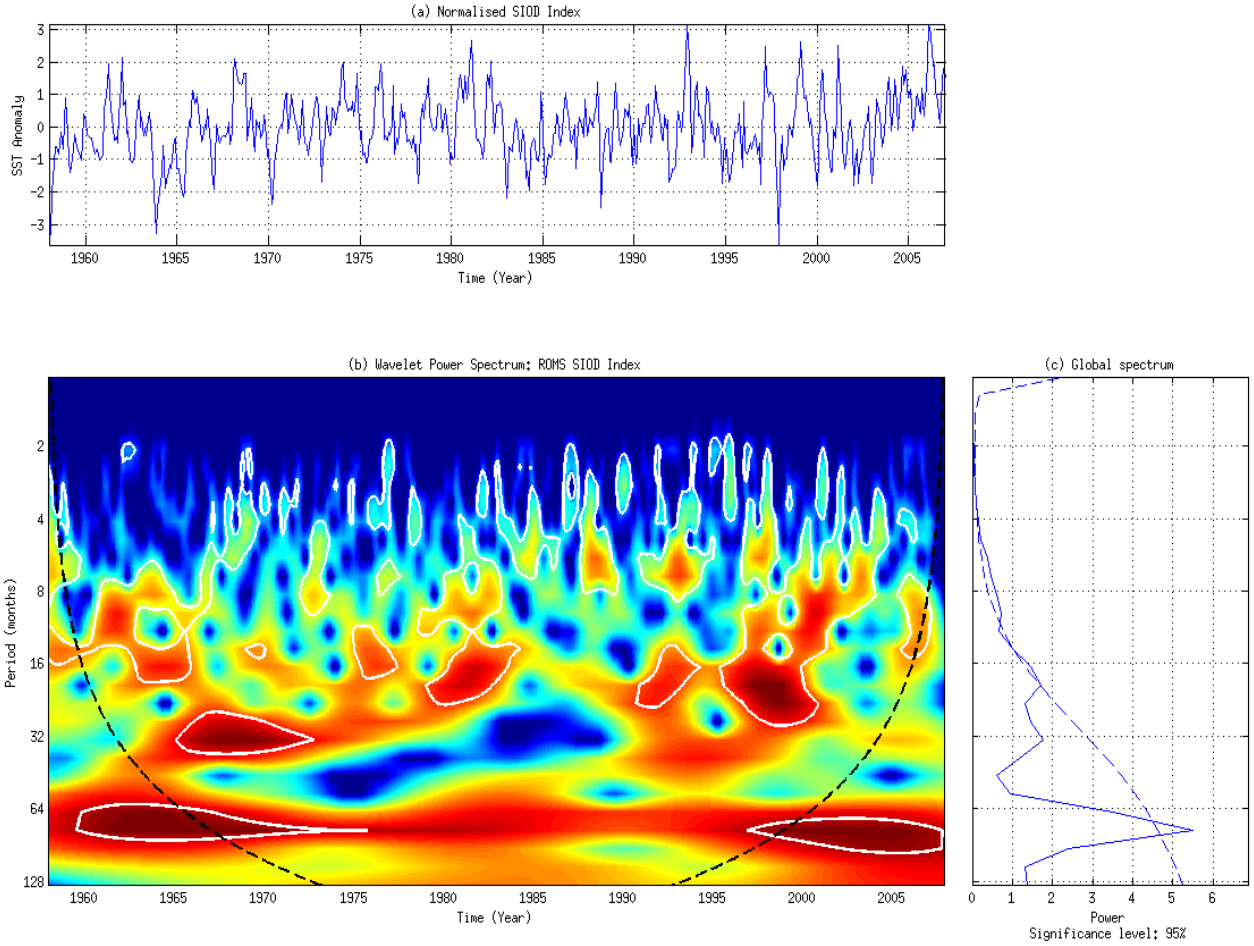

Figure 13: (a) The normalized time-series of ROMS SIOD computed from SST anomaly difference between western (55^0E-65^0E, 37^0S-37^0S) and eastern (90^0E-100^0E, 28^0S-18^0S) subtropical Indian Ocean.

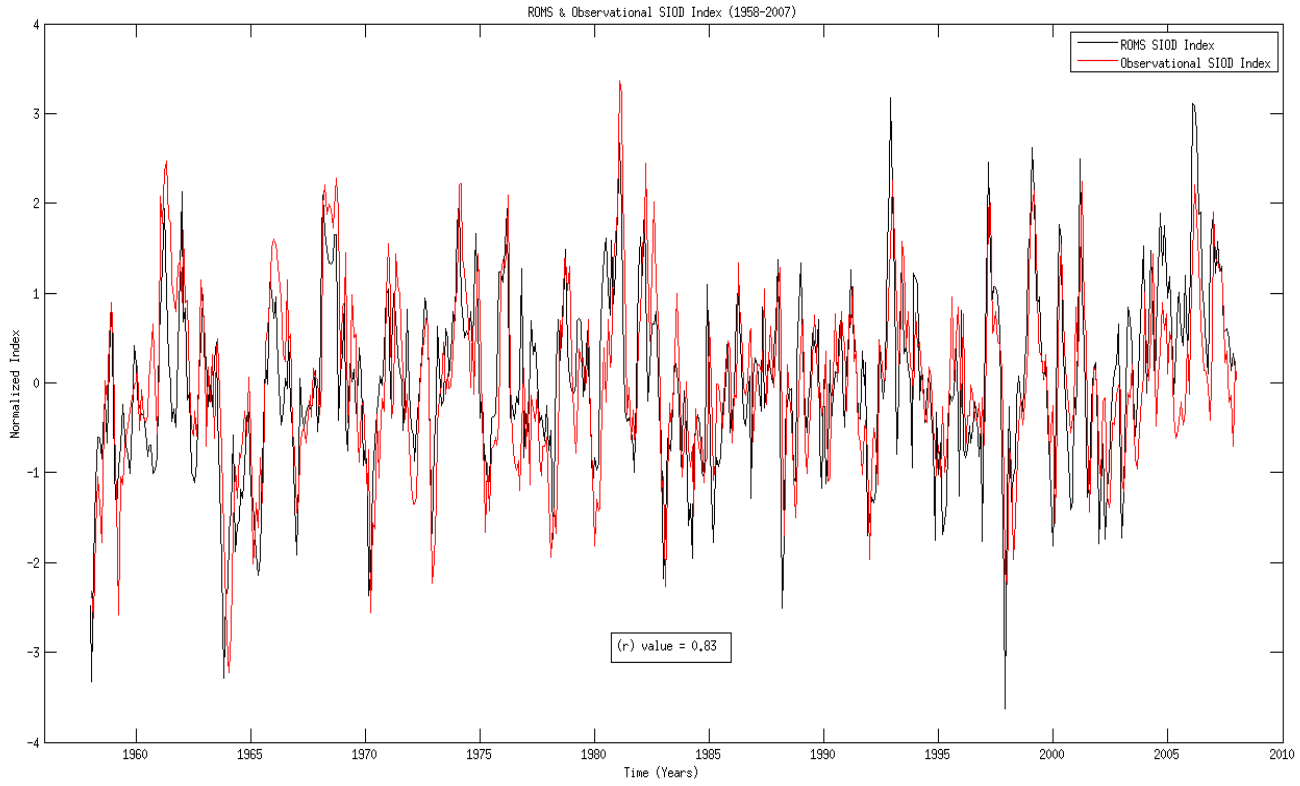

Figure 14: SIOD index calculated from ROMS (black), observations (red). These normalized indices describe the inter-annual SST variability in the subtropical Indian Ocean basin for the period 1958-2007.

4.8 Wavelet analysis of the observed SIOD Index

In this section attention is turned onto the variability of the observed SIOD index of Behera & Yamagata (2001) as that of the model SIOD index and EOF PC2 component has been presented in the previous section. At high frequency wavelet analysis results suggest that the observed SIOD index displays a semi-annual, annual and inter-annual cycles in SST. At high frequency, semi-annual periodicity is observed in the order of 4 – 12 months significant during 1960-1965, 1970-1985, and 2000. Annual periodicity was observed in the order of 14 – 24 months specifically during 1960-1985 and 1995-2000. At 32 months inter-annual periodicity was observed during the years 1965-1985 and 1993-1995 (Figure. 15). At low frequency, inter-annual variability is observed in the order of 78 months significant particularly from 1965-1985.

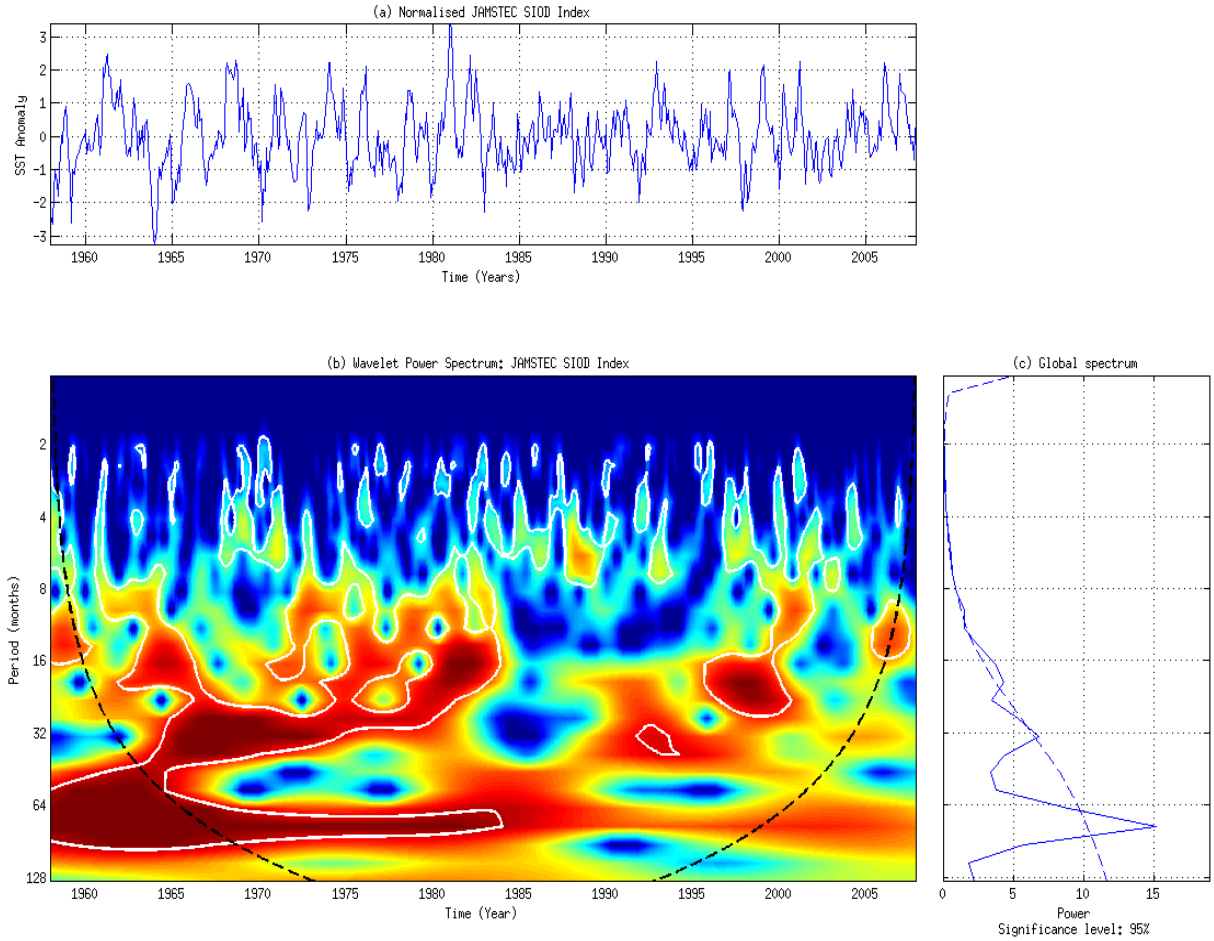

Figure 15: Anomaly difference computed from the same region as figure 12 & 13 but represents data from the observational dataset of Behera & Yamagata (2001).

4.9 SIOD Composite Map Analysis

Further investigation of the model SIOD was achieved through the use of composite map analysis with the intention was to bring out any common spatial pattern associated with a list of model positive and negative SIOD years. Individual SIOD occurrences vary in both place and time therefore the benefit of using composite maps is that they are able to highlight the main features of the events by reducing the noise of individual cases.

In this study as argued before, true dipole events occurred in those years where the absolute SDI value exceeded one standard deviation where the "dipole pattern" was oriented in a northeast-southwest direction and lastly, the polarity between the two anomaly poles must be undoubtedly clear. It must be reiterated that in this study SIOD event years were chosen by visual examination of the raw ROMS SST variability visually observing each year, and comparing them to EOF analysis spatial pattern and checking the standard deviation of the SIOD index of the potential SIOD event year. Using these criteria 12 positive and 10 negative SIOD events were identified as true dipole events years.

Positive SIOD events are noted in the years 1962, 1968, 1974, 1976, 1981, 1982, 1990, 1993, 1997, 1999, 2001, and 2006. Negative SIOD events are noted in 1958, 1964, 1970, 1972, 1975, 1983, 1988, 1995, 1998, and 2000 in agreement with Hermes & Reason (2007). The composite maps (Figures. 16, 17, 18, & 19) were then created using the above list of defined positive and negative SIOD years.

SIOD events are understood to peak during the austral summer from December to March (Figures. 16 & 17) and dissipate around May-June (Behera & Yamagata, 2001). On certain occasions however, the SIOD event do not die down completely, they revive again and to become second consecutive events such as the positive SIOD events of 1980-81 and 1981-82 (Behera & Yamagata, 2001). During positive SIOD events, cool SST anomalies are observed elongated obliquely from the eastern subtropical region to the western tropical region in the southern Indian Ocean and warm SST anomalies are observed in the region south of Madagascar (Figure. 18). The reverse is true for negative SIOD event years (Figure. 19). Figure 18 also demonstrates that during positive SIOD years the warm pole outlasts the cooler pole after the

peak season for about three months (April to June) before the pattern completely dissipates around July. The reverse can similarly be observed for negative SIOD event years (Figure. 19).

The composite difference map shows an amplified SIOD dipole pattern of SST anomalies in the SIO peaking in the austral summer and dissipating around July (Figure. 20). Positive anomalies were observed to dominate the SW region and negative anomalies were observed to be obliquely elongated from the NE subtropical region to the western tropical region of the subtropical Indian Ocean. A negative event was observed to be developing around December (Figure. 20).

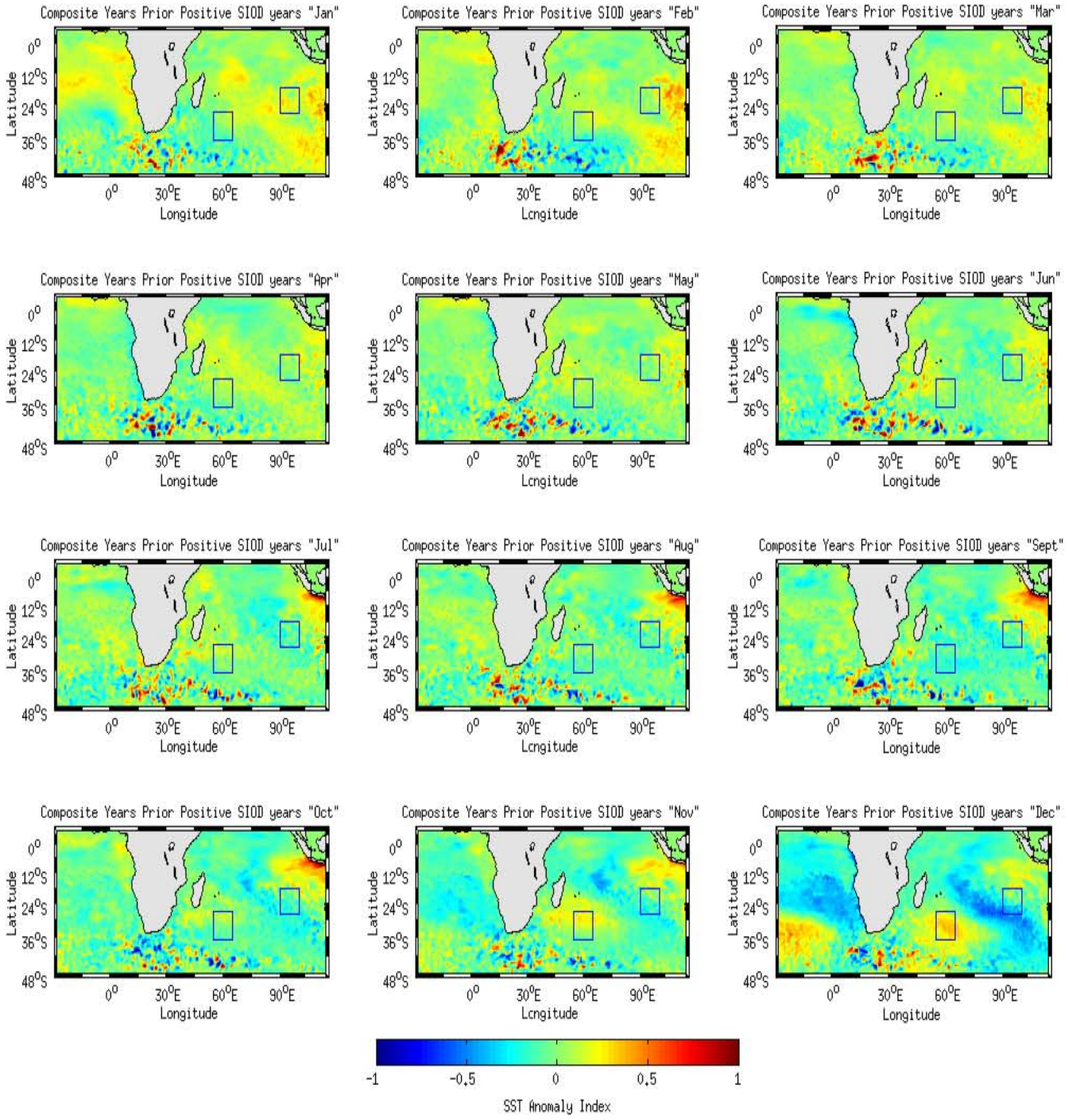

Figure16: ROMS anomalous SST prior positive SIOD event years. The boxes in blue denote the regions where the SST used to derive the SIOD index was taken.

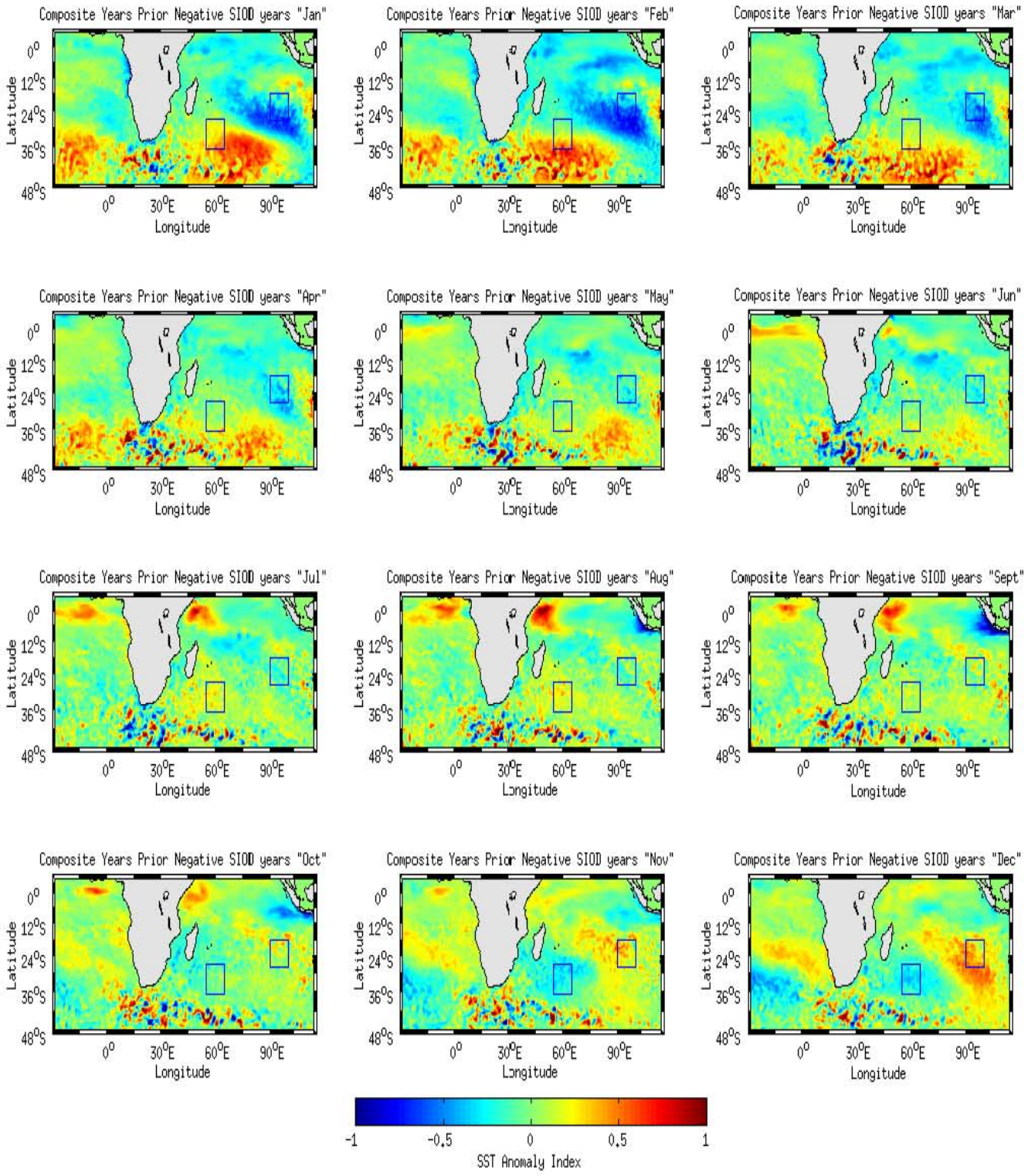

Figure 17: ROMS anomalous SST prior negative SIOD event years. The boxes in blue denote the regions where the SST used to derive the SIOD index was taken.

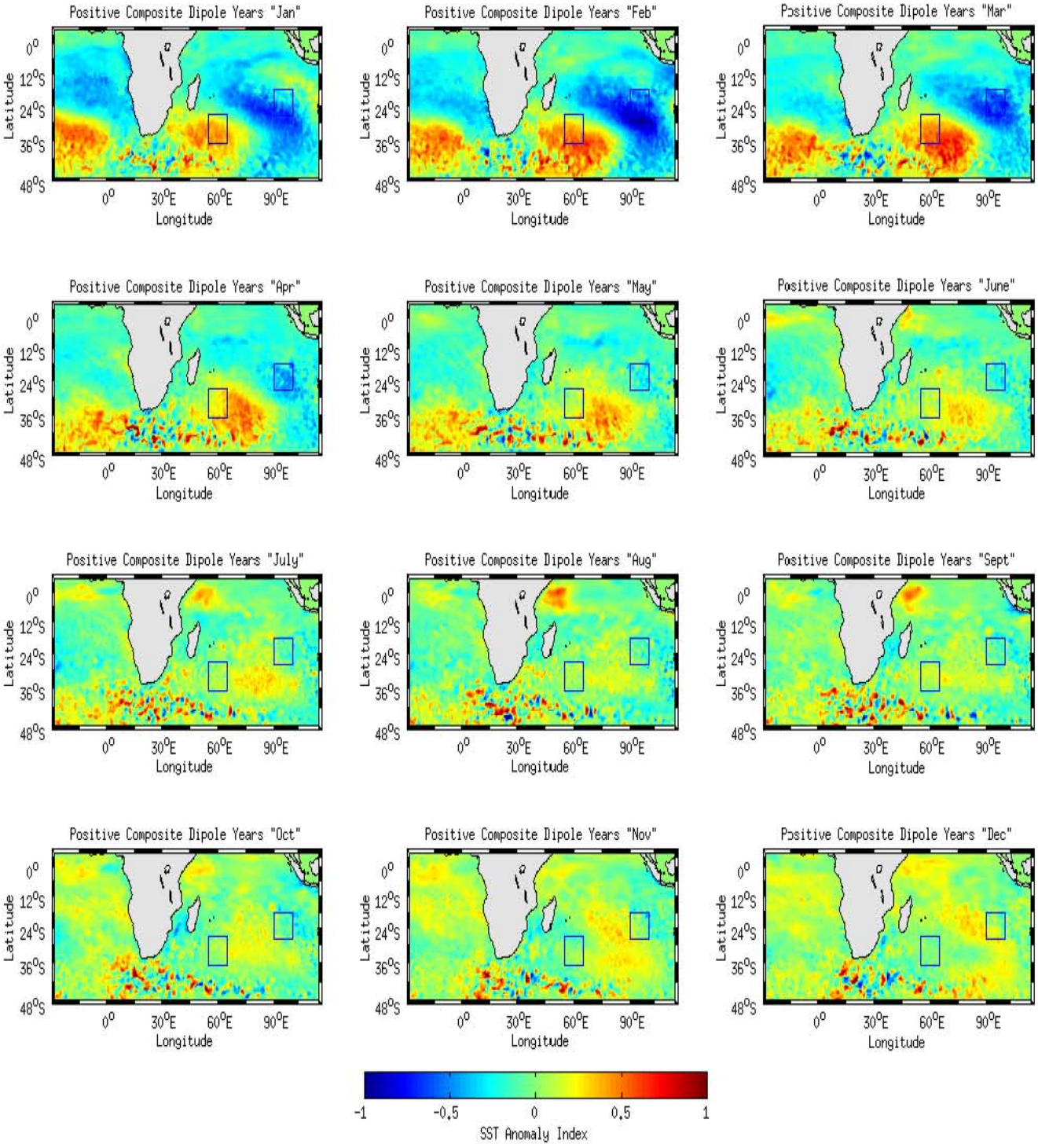

Figure 18: ROMS anomalous SST during composite positive SIOD event years (listed above). Positive SIOD event years are characterized by cool SST anomalies found elongated obliquely from the eastern subtropical region to the western tropical region and warm SST anomalies in the southeastern region of the southern Indian Ocean. The boxes in blue denote the regions where the SST used to derive the SIOD index was taken.

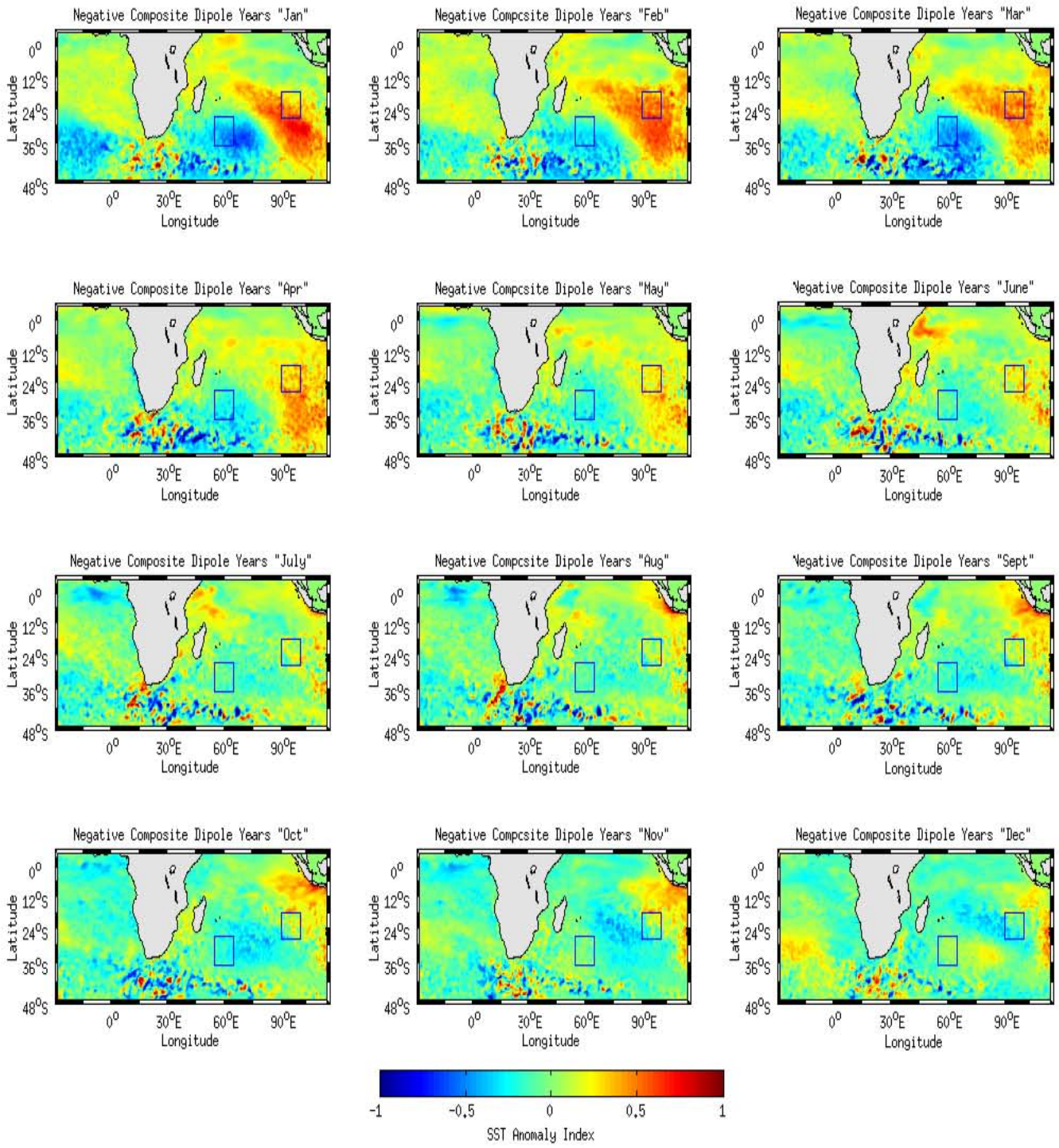

Figure 19: ROMS anomalous SST during composite negative SIOD event years (listed above). Negative SIOD event years are characterized by warm SST anomalies found elongated obliquely from the eastern subtropical region to the western tropical region and cool SST anomalies in the southeastern region of the southern Indian Ocean. The boxes in blue denote the regions where the SST used to derive the SIOD index was taken.

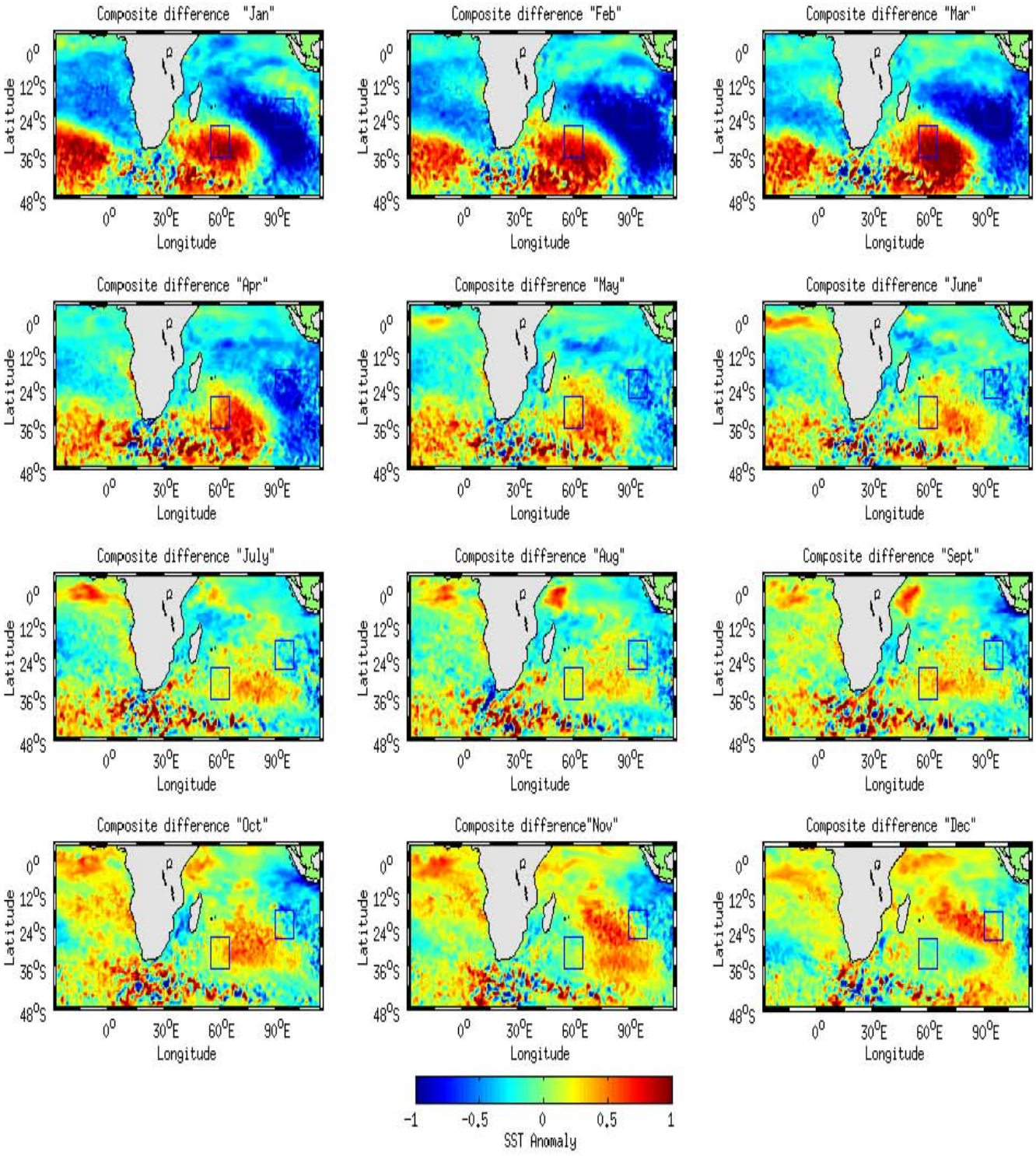

Figure 20: ROMS anomalous SST composite difference maps (Positive modes – Negative modes) for the period 1958-2007. The boxes in blue denote the regions where the SST used to derive the SIOD index was taken.

4.10 SIOD event years in the Agulhas Region during the austral summer

The previous sections have presented how the model SST compares with the WOA09 SST product and showed the usefulness of the SDI as a tool for determining the strength and phase of the SIOD. SST variability also been examined in the SIOD domain and NE and SW regions of the domain through the EOF and wavelet analysis. This chapter will explain the role shifts positive and negative modes have on the SST and SSH anomaly field in the southern Indian Ocean and Agulhas Current as well as precipitation over Africa.

Investigations of the influence model SIOD phenomenon on the SST and SSH in the Agulhas Current region have been conducted through a selection of event year composite maps. With the primary objective of this study being to ascertain whether SIOD phenomenon have an impact on the greater Agulhas Current system, this section focuses upon the time-series and composite maps of regional SST and SSH anomalies. Observing the variability of these parameters and their correlation to the SIOD index would provide further insight into the investigation of the physical links between Agulhas Current variability and SIOD events. In this case SST and SSH were chosen as the parameter to observe for changes in the characteristics of the Agulhas Current system. Positive (negative) events could be associated with a certain type of SSH and SST signal in the region.

SST and SSH variability in the Agulhas Current region (25^0E-35^0E, 30^0S-35^0S) (Figure. 3) have been examined for an influence by the SIOD events through composite map analysis and the Pearson's product moment correlation coefficient. Likewise, the geostrophic velocity at the core of the Agulhas Current (Figure. 4) has also been examined for a possible influence by the SIOD index using the Pearson's product-moment correlation co-efficient.

The figures 20 (a) & (b) display a regional account of the greater Agulhas Current SST trends during the austral summer (JFM average). Similarly, the figures 22 (a) & (b) also displays a regional account of SSH trends in the greater Agulhas Current during composite positive and negative SIOD event years. Composite difference maps are shown by figures 21 & 23 show the SST and SSH trends in the greater Agulhas Current system.

During positive SIOD years (Figure 21a) a slight anomalous warming in the Agulhas Current along the southeastern continental shelf of Africa from about 27°S to 40°S was observed. This anomalous warming observed in Agulhas Current SST appears to be connected to the warm pole of the positive SIOD through the East Madagascar Current and through the recirculation of the SW IO anticyclone into the Agulhas Current. Moreover, the region where the Agulhas Current detaches from the continental slope also shows an anomalous warming trend in SST.

An anomalous cooling trend in SST was observed in the Agulhas Retroflection Region and Agulhas Return Current. Results suggest a warming and cooling in some regions of the Agulhas Current however the anomalous behavior in SST trends during positive SIOD phenomenon is not significant due to amplitudes of the cooling or warming not being pronounced.

During negative SIOD years (Figure 21b) composite maps show that of the Agulhas Current SST trends linked to the anomalously warm SST of the warm pole of the negative SIOD event through linkages with the South Equatorial Current (SEC), connecting with the Agulhas Current through the Mozambique Channel eddies. Anomalous warming in the Agulhas Current can also be observed at the region where the Agulhas Current detaches from the continental shelf on the southeastern edge of the Agulhas Bank at approximately 30^0 E.

Furthermore, anomalous warming was observed in parts of the Agulhas Retroflection and Agulhas Return Current regions. A combination of both warming and cooling SST is observed in parts of the Agulhas Return Current in the mid-latitudes of the southern Hemisphere (Figure. 21b). To a large extent this anomalous behaviour in Agulhas Current SST during negative SIOD years was also ascertained not to be pronounced.

Composite maps of the mean austral summer Agulhas Current SSH during positive and negative SIOD years have also been shown here (Figure 23a &23b). It was observed that during positive SIOD years the region east of Madagascar is dominated by positive SSH anomalies. This anomalous positive SSH in the SW IO is evidence of an intensified Indian Ocean anticyclonic gyre during positive SIOD years. Negative SIOD years were observed to be characterized by negative SSH anomalies in the SW IO. This can be related to a relaxed Indian Ocean anticyclonic gyre during negative SIOD event years. This relaxation possibly implies weakened flows into the Agulhas Current.

Austral summer composite difference maps of Agulhas Current SST and SSH variability was also examined (Figures 22c & 24c). Composite negative SIOD event years were subtracted from composite positive SIOD event years and the output was then examined for anomalous SST and SSH behaviour in Agulhas Current.

Composite difference maps showed no significant anomalous trend in Agulhas Current SST and SSH, notwithstanding that the composite difference maps also show an anomalous warming trend in Agulhas Current SST associated with the warm pole of the positive SIOD event through linkages with the East Madagascar Current and possibly by way of the recirculation of an intensified SW IO anticyclonic gyre during SIOD events (Fig. 22c).

Anomalous warm Agulhas Current SST was also observed downstream the current in the Agulhas Retroflection Region. As observed in the composite maps similarly the composite difference maps show that the anomalous trends in SST are not pronounced and significant. Likewise, the composite difference maps of anomalous Agulhas Current SSH also suggests that SSH is also not significantly influenced by SIOD phenomenon. This was observed by the inspecting the mean SSH contours in the Agulhas Current region which did not exceed one standard deviation (Figure 24c).

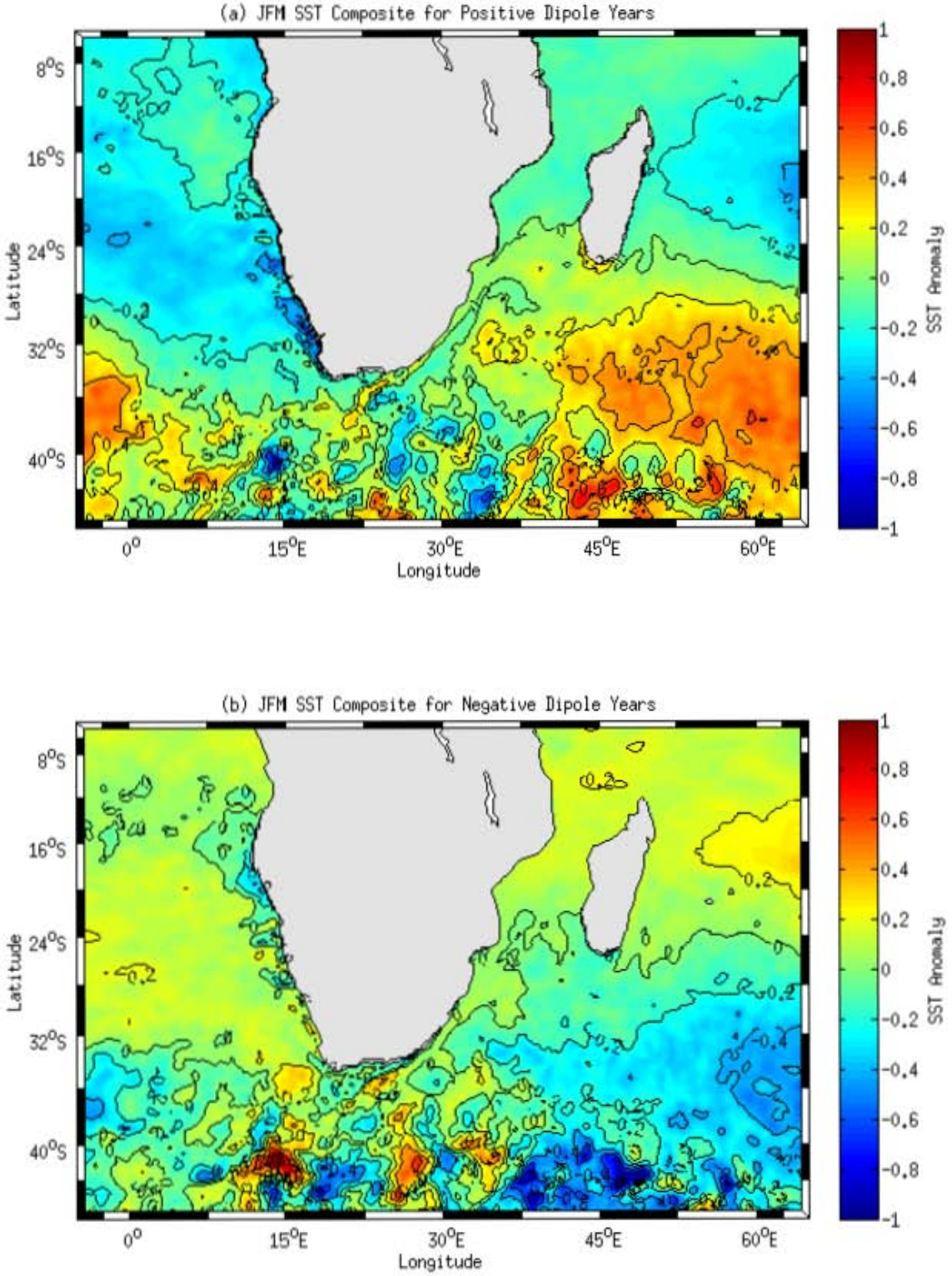

Figure 21: A zoom of model JFM SST anomalies with mean SST contours (^{0}C) during positive (a) and negative (b) SIOD events

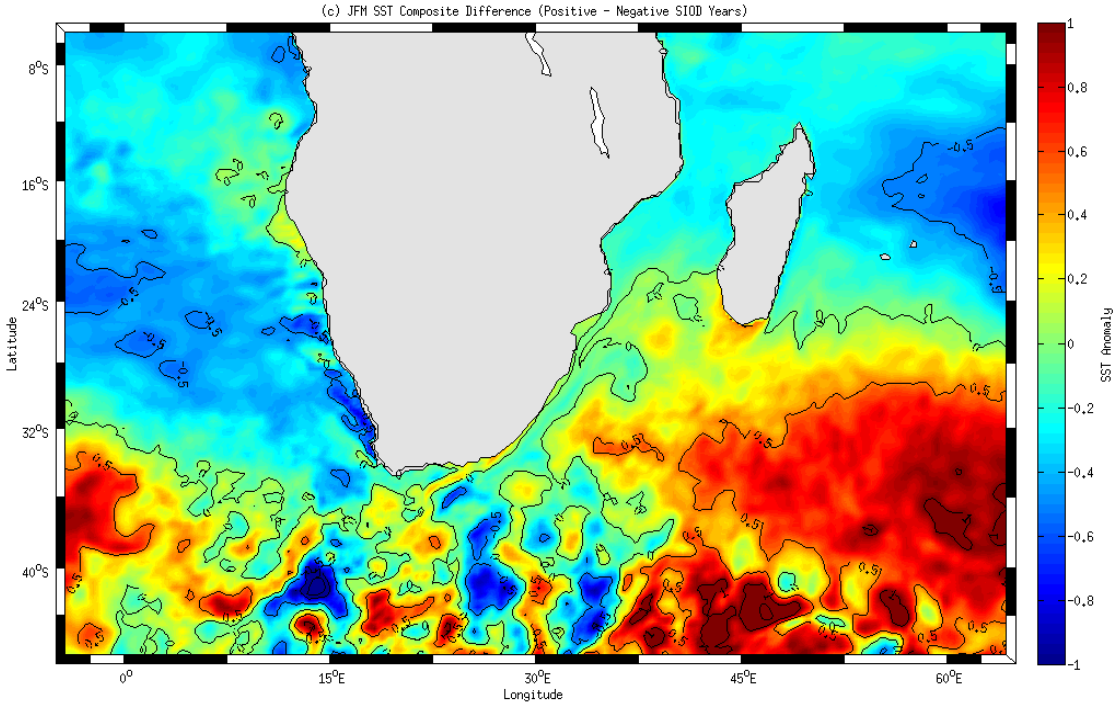

Figure 22: A zoom of the model JFM SIOD SST composite difference with mean SST contours (^{0}C).

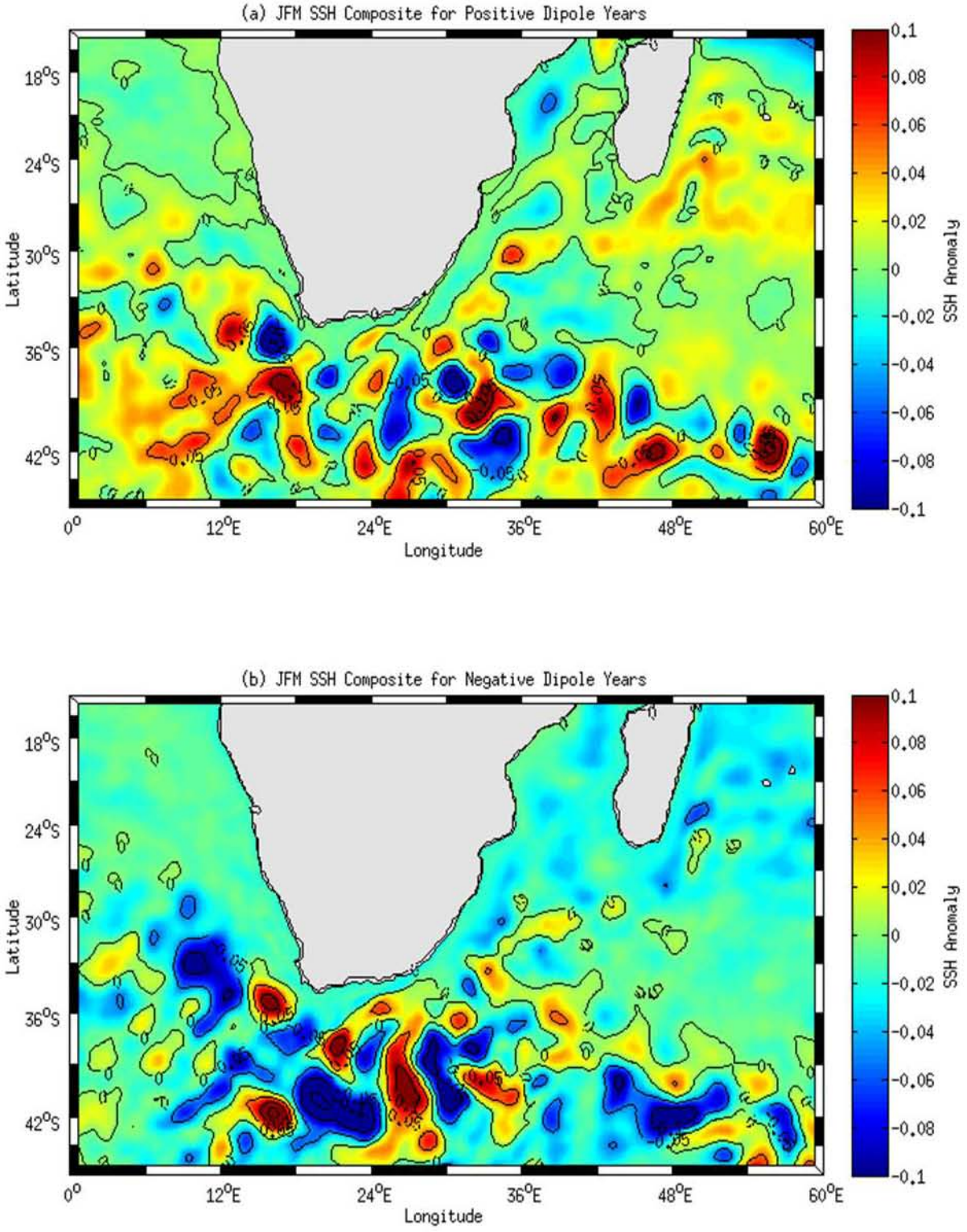

Figure 23: A zoom of model JFM SSH anomalies with the mean SSH contours (m) during positive (a) and negative (b) SIOD events

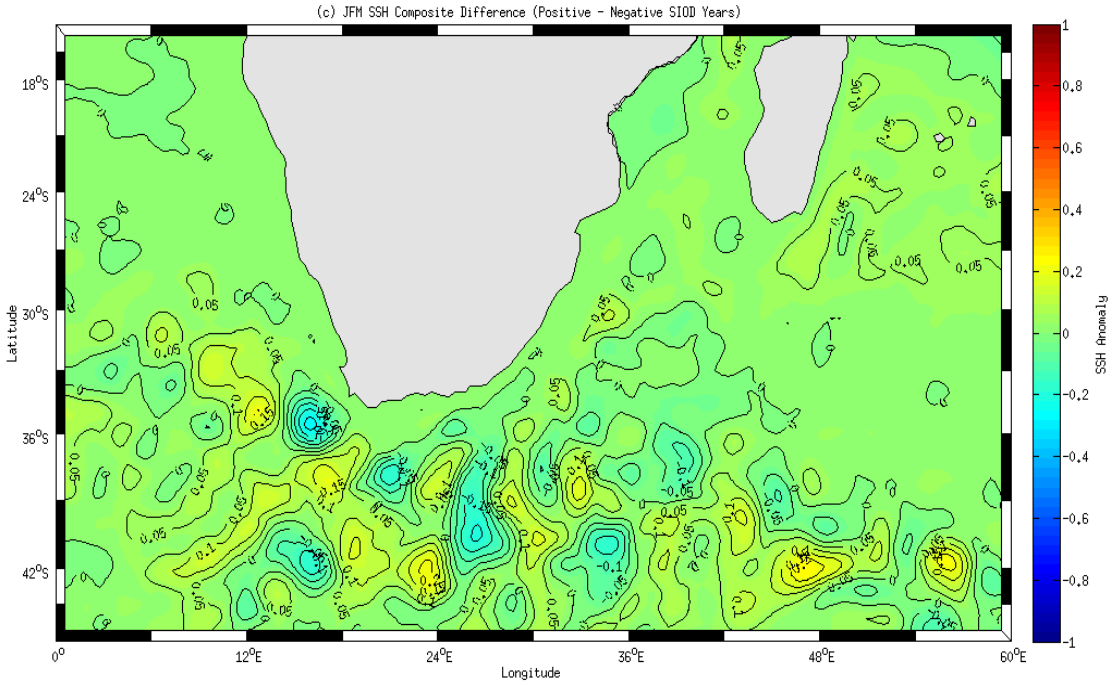

Figure 24: A zoom of the model JFM SIOD SSH composite difference with mean SSH contours (m).

4.11 Jason/Topex track #020 geostrophic velocity of the Agulhas Current

Thus far the quantitative nature of the SIOD phenomenon has been assessed using the SDI, wavelet analysis, EOF analysis, and its influence on the Agulhas Current through composite map analysis. This section will examine how the index of the geostrophic velocity of the Agulhas Current relates to SIOD events through the statistical Pearson's correlation coefficient.

Wavelet analysis applied on the satellite derived geostrophic velocities at the core of the Agulhas Current suggests a very strong annual cycle in the speed of the Agulhas Current (Krug & Tournadre, 2012). Krug & Tournadre (2012) also showed that the geostrophic current speed at the current's core exhibits distinct seasonal variations, with stronger flows observed in the austral summer (Figure. 25).

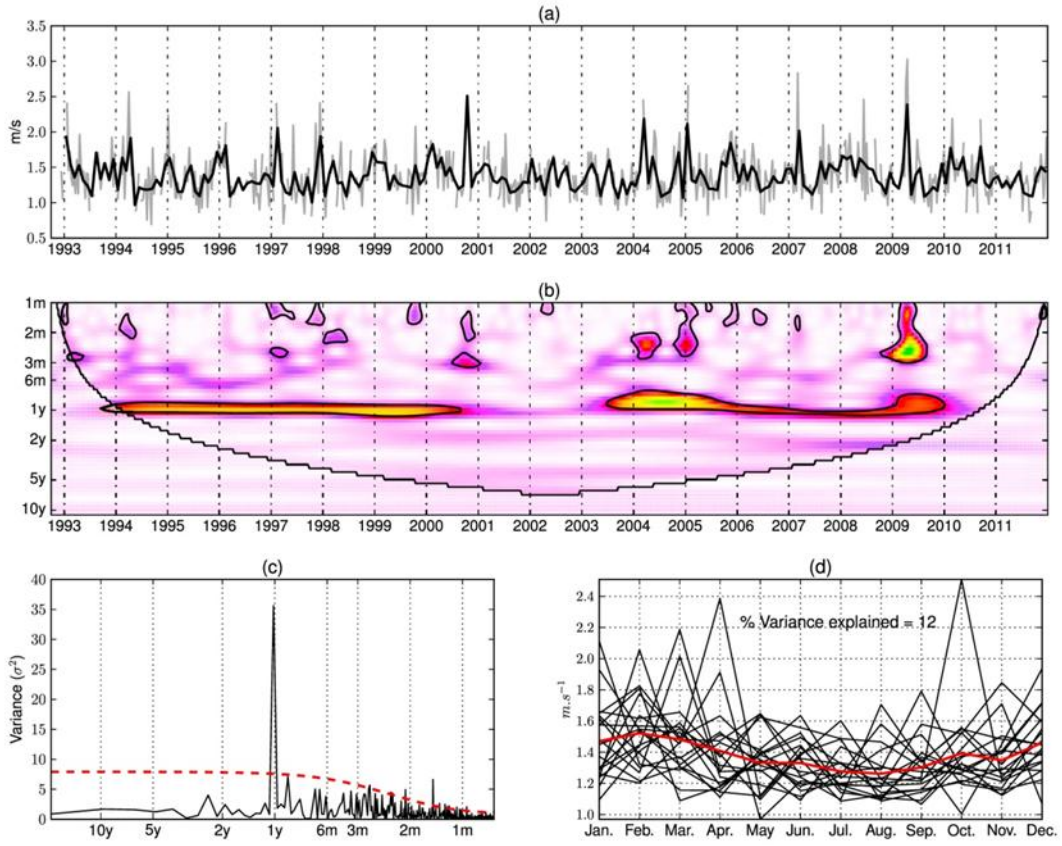

Figure 25: (a) Amplitude of the Gaussian fit to the Agulhas Current core velocities derived from the 10-day along-track altimetry (in grey). Overlaid in black are the corresponding monthly averages. (b) Continuous wavelet transform of the Gaussian fit amplitudes, with black contour lines indicating the 95% confidence interval. (c) Power frequency spectra for the Gaussian fit amplitudes, the dashed red lines indicates the 95% confidence level. (d) Monthly seasonal variations of the Gaussian amplitudes with the climatology plotted as a thick red line. Figure taken from Krug & Tournadre (2012).

4.12 Statistical correlations between climate modes and the Agulhas Current

This section will observe how other climate indices such as the anomalous ENSO index of the Pacific Ocean and anomalous IOD index of the Tropical Indian Ocean correlate with to the model SIOD index, the geostrophic velocity at the core of the Agulhas Current, and anomalous Agulhas Current SSH & SST in the region (25^0E-35^0E, 30^0S-35^0S) for the period 1958-2007 (Figure. 2 green-box). The product-moment correlation was applied to observe the relationship

between the ENSO index, the SIOD index, the geostrophic velocity at the core of the Agulhas Current and anomalous Agulhas Current SST & SSH variability (Table. 2, 3 & 4). Statistically significant *p*-values (95% confidence) are highlighted in bold. Robust correlation values here were defined as those greater than 0.5 or less than -0.5.

The relation between the observed anomalous ENSO index and the model's anomalous SIOD index of the SIO was investigated for the period 1958-2007. Visual inspection of the two graphs proposes a level of independence between the two time-series notwithstanding the fact that in-phase moments and delayed or precursor responses which could be possibly embedded. Troughs in the ENSO index observed to be in phase with troughs in the model SIOD index are in 1960, 1984, 1986, 2000 and 2003 (Figure. 26). The 0-12 month lagged correlation suggests that the ENSO index is not statistically correlated to the model SIOD index (Figure. 26 & Table. 2). The highest *r*-value for the correlation between ENSO/SIOD = -0.14 found in month 3, 4 & 5 when ENSO leads.

Likewise, the model SIOD index was plotted against the anomalous IOD index of the tropical Indian Ocean for the same period 1958-2007 (Figure. 27). The two graphs appear to be closer together possibly proposing a high level of coherence in their trends. While coherent peaks and troughs can be observed the general likelihood of a cause and effect behaviour was not shown by statistical analysis. The 0-12 month lagged correlation suggests no statistical relationship between the observed anomalous IOD signal and the model SIOD index (Figure. 27 & Table. 3).

Lastly, the satellite derived geostrophic velocity index at the core of the Agulhas Current was plotted against the model SIOD index however, for the period 1993-2007. Visual inspection of the overlaid indices suggests an inverse and proportional relationship between SIOD events years and the geostrophic velocity at the core of the Agulhas Current. Figure 28 also suggests differences in the timescale of the forcings of the indices. A high level of periodicity in the geostrophic velocities at the core of the Agulhas Current was observed. The 0-12 month lagged correlation suggested no correlation between the anomalous geostrophic velocity at the core of the Agulhas Current and the model SIOD index (Figure. 28 and Table. 4). The highest *r*-value = 0.26 when $P = 0.05$.

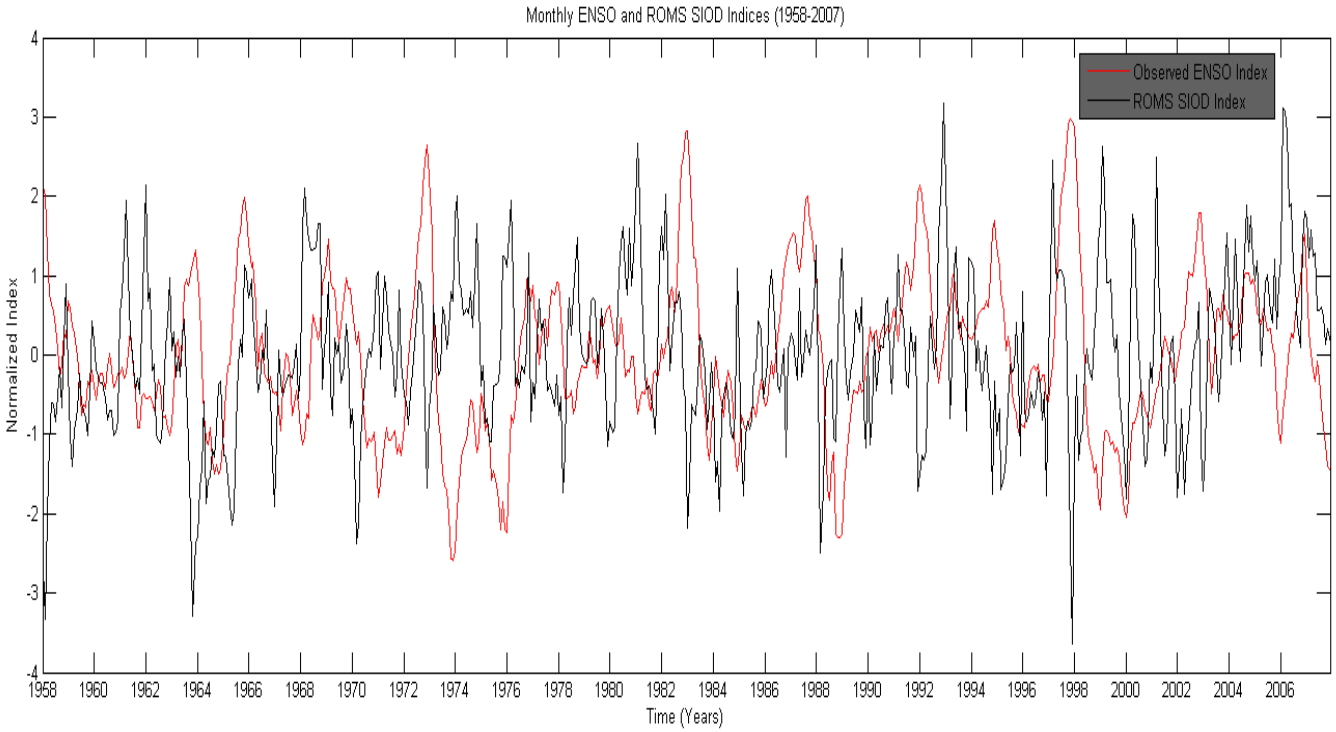

Figure 26: Anomalous ENSO index (black) and the anomalous ROMS SIOD index (red) both from 1958-2007.

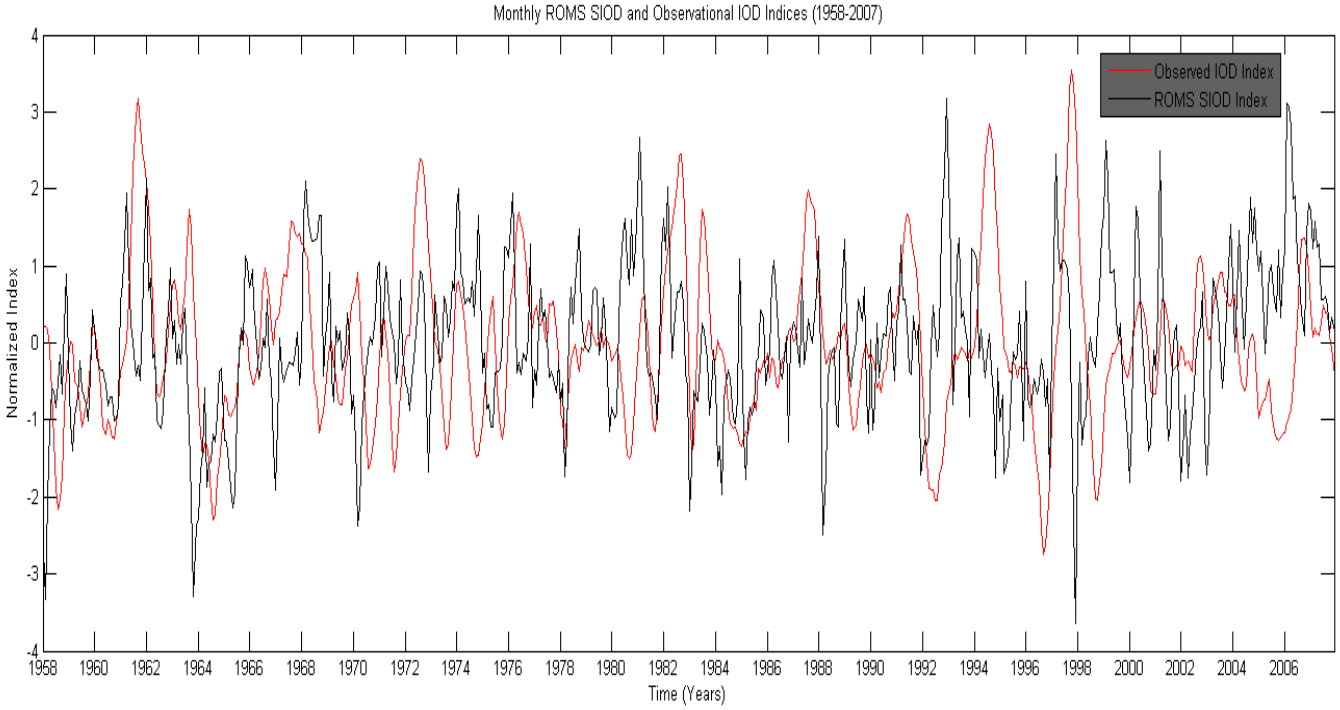

Figure 27: Anomalous ROMS SIOD index (black) and the anomalous IOD index (red) both from 1958-2007.

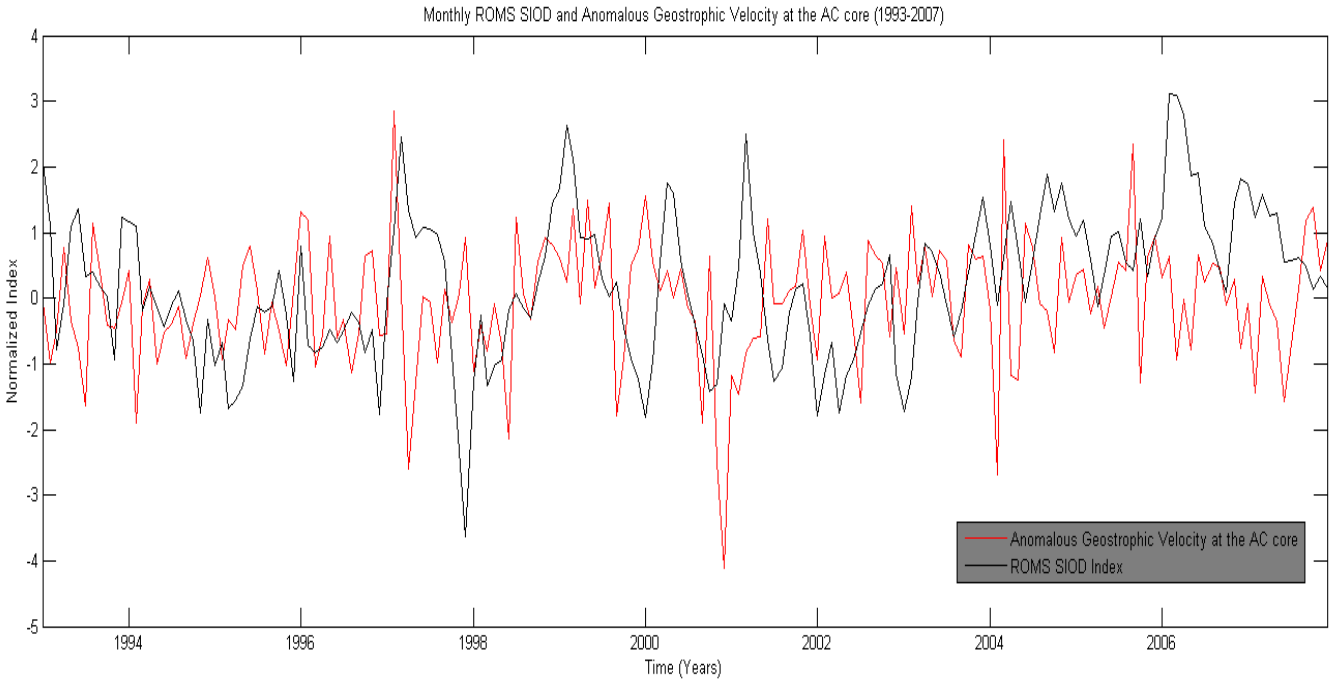

Figure 28: Anomalous ROMS SIOD index (black) and the anomalous geostrophic velocity at the core of the Agulhas Current (red) both from 1993-2007.

ENSO Index leading (months)	0	1	2	3	4	5	6	7	8	9	10	11	12
IOD Index	**0.41**	**0.39**	**0.35**	**0.31**	**0.26**	**0.21**	**0.16**	**0.10**	**0.05**	**0.01**	**-0.03**	**-0.07**	**-0.10**
SIOD Index	**-0.08**	**-0.11**	**-0.13**	**-0.14**	**-0.14**	**-0.14**	**-0.12**	**-0.11**	**-0.08**	**-0.05**	**-0.03**	**0.00**	**0.03**
EOF PC2	**-0.01**	**-0.02**	**-0.05**	**-0.07**	**-0.09**	**-0.10**	**-0.11**	**-0.11**	**-0.10**	**-0.09**	**-0.07**	**-0.06**	**-0.04**
Agulhas Current Geostrophic Velocity	**-0.24**	**-0.21**	**-0.18**	**-0.13**	**-0.07**	**-0.01**	**0.05**	**0.12**	**0.20**	**0.27**	**0.34**	**0.41**	**0.47**
Agulhas Current SST(25^0E-35^0E,30^0S-35^0S)	**-0.14**	**-0.09**	**-0.05**	**0.01**	**0.04**	**0.09**	**0.13**	**0.17**	**0.21**	**0.23**	**0.28**	**0.27**	**0.24**
Agulhas Current SSH(25^0E-35^0E,30^0S-35^0S)	**-0.04**	**-0.03**	**-0.01**	**-0.01**	**0.01**	**0.02**	**0.04**	**0.05**	**0.07**	**0.08**	**0.10**	**0.11**	**0.13**

Table 2: *R*-values of correlations between ENSO, IOD, SIOD, the second EOF PC2, geostrophic velocity at the core of the Agulhas Current, Agulhas Current SST and Agulhas Current SSH with a 0 – 12 month lag.

IOD Index leading (months)	0	1	2	3	4	5	6	7	8	9	10	11	12
SIOD Index	**0.05**	**-0.00**	**-0.05**	**-0.10**	**-0.14**	**-0.17**	**-0.18**	**-0.19**	**-0.19**	**-0.17**	**-0.16**	**-0.13**	**-0.11**
EOF PC2	**0.01**	**-0.03**	**-0.08**	**-0.13**	**-0.16**	**-0.19**	**-0.21**	**-0.22**	**-0.22**	**-0.21**	**-0.20**	**-0.18**	**-0.16**
Agulhas Current Geostrophic Velocity	**-0.36**	**-0.37**	**-0.37**	**-0.36**	**-0.33**	**-0.30**	**-0.25**	**-0.20**	**-0.14**	**-0.07**	**-0.00**	**0.06**	**0.13**
Agulhas Current SST (20E-30E, 34S-40S)	**0.01**	**0.01**	**0.01**	**0.02**	**0.02**	**0.03**	**0.05**	**0.06**	**0.08**	**0.10**	**0.12**	**0.14**	**0.15**
Agulhas Current SSH (20E-30E, 34S-40S)	**-0.07**	**-0.06**	**-0.06**	**-0.06**	**-0.05**	**-0.05**	**-0.05**	**-0.05**	**-0.05**	**-0.04**	**-0.04**	**-0.03**	**-0.03**

Table 3: *R*-values of correlations between the IOD, ROMS SIOD, the second EOF PC2 component, geostrophic velocity at the core of the Agulhas Current, Agulhas Current SST and Agulhas Current SSH with a 0 – 12 month lag.

ROMS SIOD leading (months)	0	1	2	3	4	5	6	7	8	9	10	11	12
Agulhas Current Geostrophic Velocity	**0.26**	**0.24**	**0.23**	**0.21**	**0.18**	**0.15**	**0.11**	**0.08**	**0.05**	**0.02**	**0.00**	**-0.00**	**-0.02**
Agulhas Current SST (20E-30E, 34S- 40S)	**0.11**	**0.13**	**0.15**	**0.17**	**0.19**	**0.20**	**0.21**	**0.22**	**0.22**	**0.22**	**0.22**	**0.21**	**0.20**
Agulhas Current SSH (20E-30E, 34S- 40S)	**0.28**	**0.28**	**0.28**	**0.28**	**0.27**	**0.27**	**0.26**	**0.25**	**0.24**	**0.22**	**0.20**	**0.19**	**0.17**

Table 4: *R*-values of correlations between the ROMS SIOD, second EOF PC2 component, geostrophic velocity at the core of the Agulhas Current, Agulhas Current SST and Agulhas Current SSH with a 0 – 12 month lag.

4.13 Precipitation correlations

Now that the anomalous SIOD index has been correlated to various other climate indices, attention will be now turned to the influence of the model SIOD index on southern African precipitation for the period 1979-2007. Past studies have comprehensively presented the influence of the SIOD on weather events (Reason & Mulenga, 1999; Behera & Yamagata, 2001; Reason, 2002). In this section latent heat flux anomalies and precipitation anomalies are explored in the domain (0^0S – 45^0S and 0^0 W- 110^0E) of the southern Hemisphere.

The MERRA latent heat flux anomaly for the period 1979-2007 distinctly shows that model derived SIOD index is positively correlated to latent heat flux anomalies in large regions of the Agulhas System (Figure. 28). SIOD events are observed to be linked to latent heat flux anomalies over large parts of southern African, above parts of the greater Agulhas Current System and Benguela region (Figure. 28). A large negative correlation is observed in the south eastern subtropical Indian Ocean.

The precipitation map shows SIOD index correlated to large parts of the subtropical and tropical Indian Ocean and over parts of southern Africa particularly parts of Botswana, South Africa and Mozambique in agreement with Behera & Yamagata (2001) (Figure. 29). Large negative correlations are observed in the subtropical regions and mid-latitudes of the south Atlantic. In the subtropical Indian Ocean a large significant negative correlation is observed obliquely stretched similar to the orientation of the eastern pole of SIOD events in the subtropical Indian Ocean (Figure. 29). The intensity of the correlation coefficient for both latent heat flux and precipitation anomalies was observed to decrease over time.

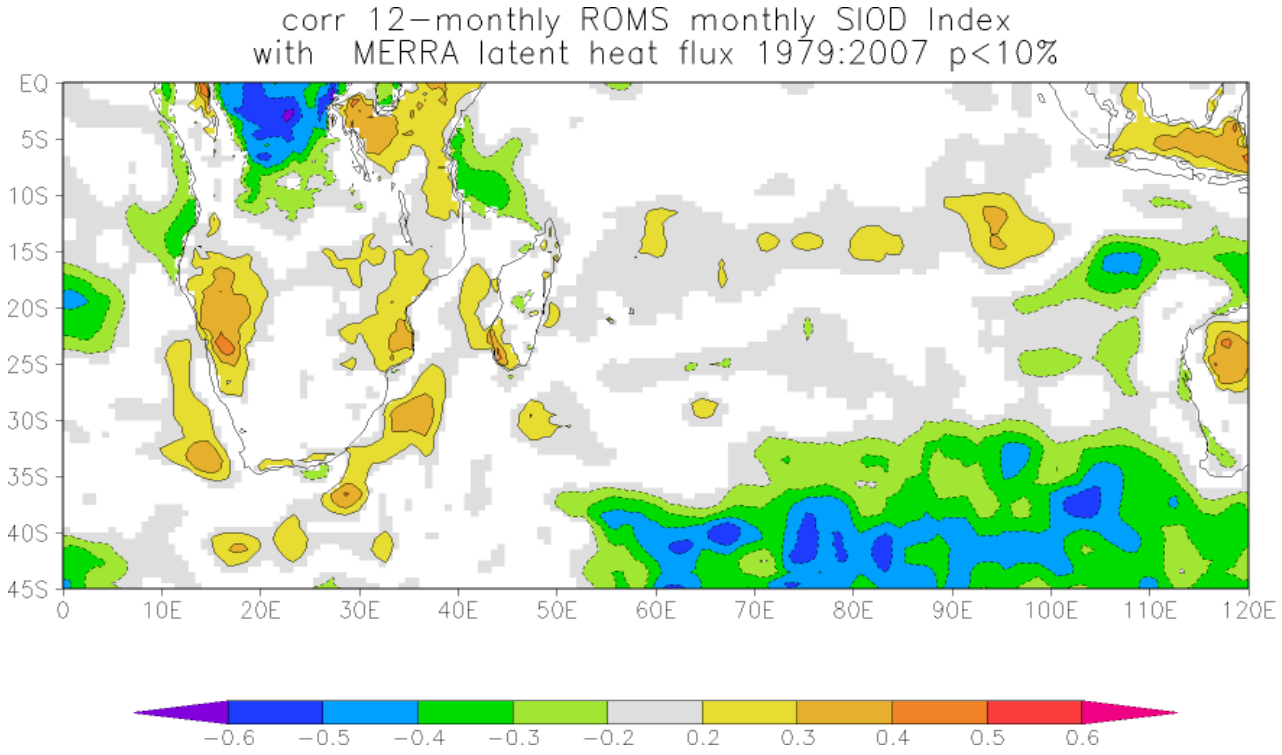

Figure 29: 12 month average NASA MERRA reanalysis latent heat flux anomalies (1979-2007) correlated to them ROMS model SIOD index at 0 lag.

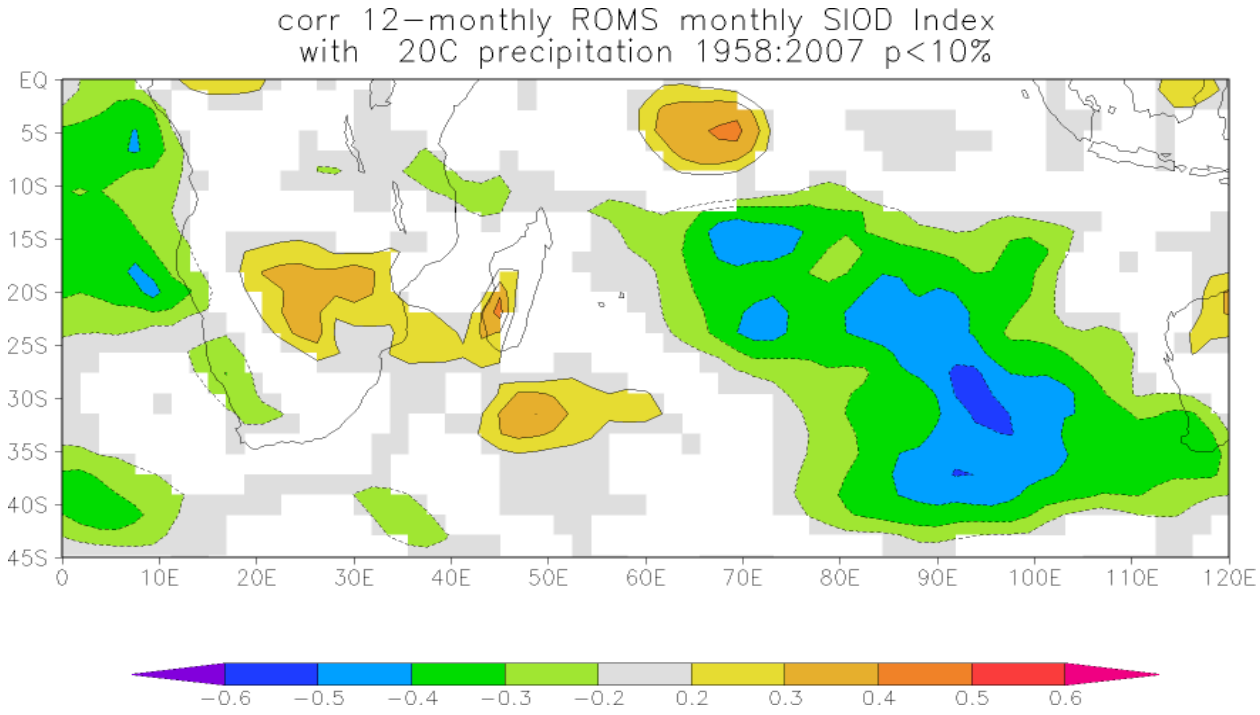

Figure 30: 12 month average NCEP-NCAR twentieth century reanalysis precipitation anomalies (1979-2007) correlated to them ROMS model SIOD index at 0 lag.

5 Discussion

This study set out to investigate the influence of the SIOD phenomena on the Agulhas Current with particular reference to the geostrophic velocity at the core of the Agulhas Current and Agulhas Current SST and SSH variability. The hypothesis argued here relates characteristics of SIOD events in the subtropical Indian Ocean to those of IOD phenomenon of the tropical Indian Ocean. The objective was to assess how SIOD events influence the Agulhas Current.

In this study the ROMS SIOD phenomena emerged as the second EOF mode in the SIO in agreement with observations in Behera & Yamagata, (2001); Qian *et al*. (2002); and Suzuki *et al*. (2004). It was also shown that SIOD events and phases are non-linearly related to each other and the ENSO index, the IOD index, the SIOD index, Agulhas Current core speeds, and Agulhas Current SST and SSH.

5.1 Subtropical Indian Ocean variability

Short and long term variability of SIO SST has been linked to the variability of other large scale climate modes and Hermes & Reason (2005) linked decadal variability in SIO SST to the Antarctic Oscillation, which seems to have strengthened after the mid-1970s. Reason & Rouault (2009) suggest that on decadal time scales, ENSO-like decadal variability and/or the Pacific Decadal Oscillation (PDO) possibly exerts an influence on IO SST variability and atmospheric circulation. Modulations of the subtropical anticyclone may also lead to changes in the tropical easterlies and mid-latitude westerlies in both the South Atlantic and South Indian Oceans leading to an influence on the anomalies of latent heat fluxes, upwelling, and Ekman heat transports, all of which contribute to the SST variability.

Wavelet analysis results suggest SST anomalies in the NE and SW IO regions demonstrate periodicities in both the high and low frequency part of the spectrum. Only the NE region of the SIO displayed low frequency variability in the order of 78 months. The SW region of the SIO did not show any low frequency periodicity. These trends were investigated by examining the anomalous time-series and wavelet analysis of the NE and SW IO for the period 1958-2007. In

the high frequency, the NE IO SST demonstrated significant semi-annual to annual and inter-annual periodicity in the order of 5-12 and 15-24 months. These timescales coincide with the inter-annual variability of the subtropical anticyclone. NE IO SST variability to some extent may also be controlled by the trade winds. In future studies the impact of the monsoon on the SIOD investigated SST can also be investigated.

The SW region's SST variability demonstrated greater variability in comparison to the NE IO. SST variability in the SW IO comprised of only high frequency semi-annual to annual periodicity in the order of 4-15 months. SST variability in this region could be intricately linked to the high frequency variability of other systems in the southern Hemisphere such as the southern Hemisphere westerlies, possibly the IOD through the transport of equatorial waters to the subtropics and mid-latitudes through the SEC, the flow east of Madagascar and through the recirculation of the Indian Ocean gyre at various timescales. Further investigation into this is required but was outside the scope of this study. At seasonal timescales southern Hemisphere westerlies may have an anomalous strengthening (weakening) impact on the wind field above SW IO and that should directly affect SST in the region. It then follows that Ekman transport proceed with surface mixing processes which may play active roles in the controlling the inter-annual variability of SIOD SST. (Hermes & Reason, 2005).

5.2 EOF Analysis

Model EOF results showed the SIOD phenomenon oriented in the northeast-southwest direction as the second EOF mode explaining 8.93% of the total variance in the SIO. Kataoka *et al.* (2012) used control runs of 22 twentieth century CGCMs submitted to the Coupled Modeling Inter-comparison Project (CMIP3) (Meehlet *et al*. 2007) where EOF analysis on both observation and model outputs showed that 13 models out of the 22 models captured the SIOD as the second EOF mode while some cases the captured SIOD events as the first mode.

An ENSO relationship with the first EOF mode has been suggested by Hermes & Reason (2005). The second EOF mode is influenced by neither ENSO nor the IOD as shown by the lag

correlations on Table 2 & 3. EOF results also suggested that the model SIOD signal is strongest during the austral summer (JFM).

EOF analysis applied on only austral summer months emerged the dipole pattern as the first mode of variability, explaining 20.84% of the total variance, furthermore, the model EOF PC2 component showed a strong correlation with the SIOD index (*r = 0.91)*

5.3 Agulhas Current Composites

Composite map results showed that SIOD events have no significant influence on the Agulhas Current SST & SSH variability. Both composite positive and negative SIOD events did not show a significant influence on the Agulhas Current notwithstanding that anomalous SST was observed in the Agulhas Current SST during negative and positive SIOD event years. The variations were observed to be not statistically significant.

During positive SIOD years a slight anomalous warming in the Agulhas Current along the southeastern continental shelf of Africa from about 27°S to 40°S was observed. This anomalous warming appeared to be connected to the warm pole of the positive SIOD through the East Madagascar Current and through the recirculation of the SW IO anticyclone into the Agulhas Current however these trends were not pronounced or significant.

During negative SIOD years composite maps showed that the Agulhas Current SST trends are linked to anomalously warm SST of the warm pole of the negative SIOD event through linkages with the South Equatorial Current (SEC), connecting with the Agulhas Current through the Mozambique Channel eddies however these trends were not pronounced or significant.

The study has also shown that during positive SIOD years the region east of Madagascar is dominated by positive SSH anomalies. These anomalies were evidence of an intensified Indian Ocean anticyclonic gyre observed during positive SIOD years. Negative SIOD years were observed to be characterized by negative SSH anomalies in the SW IO which were related to a relaxed Indian Ocean anticyclonic gyre observed during negative SIOD event years. This intensification and relaxation could possibly have implications on the magnitude and direction of

the mean flow of the Agulhas Current, however, composite difference maps showed that the anomalous trends in SST and SSH are neither pronounced nor significant.

5.4 Correlations

The model derived SIOD index did not show any significant statistical correlation with ENSO, the IOD and satellite derived geostrophic velocity at the core of the Agulhas Current as suggested by investigations of 12 month lagged correlations showing that the SIOD signal neither affects Agulhas Current SST nor SSH. SIOD phenomena are independent of Pacific Ocean climate modes and tropical Indian Ocean climate mode variability. To a large extent the evolution of SIOD phenomena has been linked to various other phenomena such as the subtropical anticyclone, MLD, and near surface humidity dynamics.

Rouault *et al*. (2009) argued that an augmentation of the transport and warming of the Agulhas Current is primarily due to increased wind stress curl in the south Indian Ocean at relevant latitudes. This result lends credence to the fact that the Agulhas Current is primarily driven by positive wind stress curl over the subtropical Indian Ocean and the main controls on retroflection and leakage are the westerlies (Beal *et al*. 2011). It then seems the Agulhas Current variability is not influenced by the SIOD rather the main controls to a large extent are the trades, westerlies and wind stress curl (Durgadoo *et al.* 2013).

Anomalous precipitation and latent heat flux anomalies correlate well with the SIOD index above parts of the southern African continent and Western Australia. The anomalous precipitation pattern correlates significantly with the anomalous SIOD index. The influence of SIOD phenomena on the summer rainfall patterns of the surrounding regions of coastal eastern South Africa, Mozambique, Zimbabwe and Botswana is shown (Behera & Yamagata, 2001; Reason, 2001, 2002). The mechanism behind the influence on weather has been explained by Reason (2001) as being that during positive SIOD events increased evaporation occurs over the southwestern warm pole and this moist air is then advected towards the southern African continent where convergence take place and anomalous precipitation events follow. Similarly, negative SIOD events influence southern African weather events by reducing precipitation on the

adjacent southern African continent due to suppressed evaporation above the cooler SST pole (Behera & Yamagata, 2001).

The key questions asked by this study included an investigation of whether the ROMS ARC configuration in (Loveday *et al.* submitted) with a particular resolution increase around South Africa was capable of producing SIOD phenomena with characteristics comparable to those of observational SIOD datasets. The EOF and composite map analysis simulations showed that the model has a very skill in producing SIOD events. The model SIOD index and EOF PC 2 component displayed a high correlation with the observational SIOD implying that the model can be trusted to faithfully reproduce the SIOD events of the SIO. Therefore the model was used to investigate the SIOD phenomena.

Regarding model SIOD phenomena time-scales of variability the observational SIOD index dataset and model SIOD SST periodicities were observed to display similar periodicities. Through wavelet analysis the NE IO region of the SIO was observed to have significant dominant periodicities in both the high and low frequency part of the spectrum whereas the SW IO region exhibited only high frequency periodicity. These periodicities however were not observed to influence or force the annual cycle of the Agulhas Current. Furthermore, no statistical correlation was found between the SIOD index and the geostrophic velocity at the core of the Agulhas Current Agulhas Current. No connection was found positive and negative SIOD events on anomalous Agulhas Current SST and SSH variability.

6. Conclusion

A ROMS based investigation of the influence of SIOD phenomena on the Agulhas Current and on SIO features was conducted. Role shifts in positive and negative modes were hypothesized to have an influence on the Agulhas Current variability mainly through modulations of the wind which are expected play a role major role in current velocity and direction. ROMS was used here as the ARC model configuration (Loveday *et al.* submitted) which is an eddy permitting implementation of ROMS constructed using ROMSTOOLS (Penven *et al*. 2008). The model has a horizontal resolution of ¼ of a degree, with an Arakawa-C Mercator grid extending from 29°W to 115°E and from 7°N to 48.25°S.

The model SST field was validated using data from the 2009 World Ocean Atlas (WOA) product. The model exhibited a warm temperature bias near the equator, furthermore, the model tended to overestimate the spatial spreading of the 28^0 isotherm. A meridional SST gradient of approximately 0.0025°C per km in WOA09 and 0.0027°C per km in ROMS was observed as one moves from the equatorial region to approximately 45°S of the SIO. The Agulhas Current in the model was also identified by the steep SST gradient of about 10°C $(100km)^{-1}$ according to Rouault *et al.* 2002 offshore the east coast of South Africa between the current and surrounding ocean. Models have constraints in terms of reanalysis data, resolution and higher levels of parameter variability and the fact that bulk forced ocean-only models such as the one used here are constrained towards (the given) atmospheric temperature. In consequence the SST is not able to freely evolve and remains dampened. Because of the great complexity of the dynamic earth system ocean-atmosphere models are better suited at representing realistic changes in climate forcings.

ENSO was examined for an influence on IOD through atmospheric teleconnections leading which could possibly lead to downstream modulations of the Agulhas Current through volume transport dynamics. Through EOF analysis the model described SIOD events as the second mode of variability in the SIO which develop around December and peak in the austral summer. During the austral summer it was shown that the SIOD becomes the leading mode of variability in the SIO. No correlation could be established between the ENSO and the IOD. Furthermore,

SIOD phenomena did not show any links with other remote forcings such as ENSO and the IOD. Composite maps of positive and negative SIOD years indicated no significant anomalous behaviour in Agulhas Current SST and SSH in response to mode shifts of the SIOD phenomenon. Moreover, the geostrophic velocity at the core of the Agulhas Current which is satellite derived and thus has inherent limitations showed no statistical correlation with SIOD, IOD and ENSO events.

Agulhas Current SST, SSH and geostrophic velocity variability did not show any significant cause and effect relationship with the SIOD index and other large scale climate modes in the Indian and Pacific Oceans. SIOD events were nonetheless observed to be correlated to anomalous precipitation in large areas of southern Africa and the subtropical Indian Ocean. This study has argued that SIOD phenomena do not appear to neither affect Agulhas SST and SSH variability nor speeds at the core of the Agulhas Current. However, this needs to be further examined, in particular by performing a more in-depth analysis with the model data.

As a reference for future work an analysis of the dynamical ocean circulation would require a closer look into deeper hydrographic and circulation fields. Future research can focus also on the influence of the SIOD phenomena on the transport values through a defined vertical section of the Agulhas Current through observational (currently very limited) and model studies. Investigating the relationship between transport values from moored data across the Mozambique Channel and possibly East Madagascar to shifts in SIOD and IOD would also help to understand the influence of the SIOD on the variability in the Greater Agulhas Current system.

It was beyond the scope of this study to assess other seasonal to decadal phenomena in the southern Hemisphere that could have an influence on the SIOD such as Madden-Julian Oscillation, the westerlies and trades. Given the evidence that the variability of the Agulhas Current is driven by the positive wind stress curl over the subtropical Indian Ocean there is potentially a more complex relationship between the Agulhas Current, the SIOD and large scale variability. This thesis has aimed to use model and satellite data to perform the steps towards improving our understanding of the relationship between the Agulhas Current and large scale SIO variability, and although significant correlations were found, interesting questions have been raised which can used to derive future research.

References:

Ash, K. D. & Matyas, C. J., 2012: The influences of ENSO and the subtropical India Ocean tropical cyclone trajectories in the southwestern Indian Ocean. International Journal of Climatology, [Online], 32, 41–56.

Beal, L.M., P.M. De Ruitjer, A. Biastoch., R. Zahn and SCOR/WRCP/IAPSO Working Group 136*, 2011: On the role of the Agulhas system in ocean circulation and climate. Nature, Vol. 472, 429-436

Behera, S. K. & Yamagata, T., 2001: Subtropical SST dipole events in the southern Indian Ocean. Geophysical Research Letters. 28, 327–330.

Biastoch, A., Reason, C.J.C., Lutjerharms, J.R.E. & Boebel, O., 1999: The importance of flow in the Mozambique Channel to seasonality in the greater Agulhas Current System. Geophysical Research Letters. 26, 3321-3324

Bryden, H.L., Beal, L.M. & Duncan, L.M., 2005: Structure and transport of the Agulhas Current and its temporal variability. Journal of Oceanography.

Carton, J. A., Chepurin, G., Cao, Z & Giese, B., 2000: A simple ocean data assimilation analysis of the global upper ocean 1950-95. Journal of Physical Oceanography, 30, 294-309.

Chiodi, A.M. & Harrison, D.E., 2007: Mechanisms of Summertime Subtropical Southern Indian Ocean Sea Surface Temperature Variability: On the Importance of Humidity Anomalies and the Meridional Advection of Water Vapor. American Meteorological Society, 20,4835-4852.

Comiso, J., 2009: Polar Oceans from Space. 1st ed. London. Springer New York Dordrecht Heidelberg London.

Compo, G.P., Whitaker, J.S., & Sardeshmukh, P.D., 2008: The 20th Century Reanalysis Project. In: Proceedings of the Third WCRP International Conference on Reanalysis. Japan, The University of Tokyo 28 Jan-1 Feb 2008.

Debreu, L., Vouland, C., & Blayo, E., 2008: Agrif: Adaptive grid refinement in Fortran. Computers & Geosciences, 34, p.8.

De Ruitjer, W.P.M., Biastoch, A., Drijfhout, S.S., Lutjerharms, J.R.E., Matano, R.P., Pichevin, T., van Leeuwen, P.J., & Weijer, W., 1999: Indian-Atlantic inter-ocean exchange: dynamics, estimation and impact. Journal of Geophysical Research, 104(C9): 20,885-20,911.

De Ruitjer, W.P.M., van Leeuwen, P.J., & Lutjerharms, J.R.E., 1999: Generation and evolution of Natal Pulses: solitary meanders in the Agulhas Current. Journal of Physical Oceanography, 29(12): 3043-3055.

Donohue, K.A., Firing, E., & Beal, L., 1999: Comparison of three velocity sections of the Agulhas Current and Agulhas Undercurrent. Journal of Geophysical Research, 105 (C12), 585-593.

Durgadoo, J.V., Loveday, B.R., Reason, C.J.C., Penven, P., Biastoch, A., 2013: Agulhas Leakage Predominantly Responds to the Southern Hemisphere Westerlies. Journal of Physical Oceanography, 43, 2113-2131.

Fairall, C., Bradley, E., Rogers, D., & Edson, J., 1996: Bulk parameterization of air-sea fluxes for tropical ocean-global atmosphere coupled-ocean atmosphere response experiment. Journal of Geophysical Research, 101 (C2), 3747–3764.

Fauchereau, N., Tzaska, S., Richard, Y., Roucou, P., & Camberlin, P., 2003: Sea-surface temperature co-variability in the southern Atlantic and Indian Oceans and its connections with the atmospheric circulation in the southern hemisphere. International Journal of Climatology, 23, 663–677.

Fowler, A.M., 2005: Sea-level pressure composite mapping in dendroclimatology: advocacy and an Agathis australis (kauri) case study. Climate Research, 29, 73-84.

Goddard, L., & Graham, N. E., 1999: Importance of the Indian Ocean for simulating rainfall anomalies over eastern and southern Africa. Journal of Geophysical Research, 104, 19 099–19 116.

Grundlingh, M.L., 1983: On the course of the Agulhas Current. South African Geographical Journal, 65(1) 49-57.

Haidvogel, D.B., & Beckmann. A., 1999: Numerical Ocean Modelling. London: Imperial College Press.

Harris, T.F.W, Legeckis, R., & van Forest, D., 1978: Satellite infra-red images in the Agulhas Current system. Deep Sea Research, 25(6): 543-548.

Hermes, J.C. & Reason, C. J. C., 2005: Ocean model diagnosis if interannual coevolving SST variability in the southern Indian and south Atlantic Oceans. Journal of Climate, 18, 2864–2882.

Hermes, J.C., Reason, C.J.C., & Lutjerharms, J.C.R., 2007: Modeling the Variability of the Greater Agulhas Current System. American Meteorological Society, 20, 3131-3144.

Huang, B. & Shukla, J., 2007: Mechanisms for the Interannual Variability in the Tropical Indian Ocean. Part II: Regional Processes. American Meteorological Society, 1. 2937-2959.

Kataoka, T., Tozuka, T., Masumoto, Y. & Yamagata, T., 2012: The Indian Ocean subtropical dipole mode simulated in the CMIP3 models. Climate Dynamics, 39,1385-1399.

Krug, M.J. & Tournadre, J., 2012: Satellite observations of an annual cycle in the Agulhas Current. Geophysical Research Letters, 39, L15607.

Large, W. & Yeager, S., 2004: Diurnal to decadal global forcing for oceans and sea-ice models: the data sets and flux climatologies. NCAR Technical Note, 1–112.

Locarini, R. A., Mishonov, A.V., Antonov, J.I., Boyer, T.P. and Garcia, H.E., 2006: World Ocean Atlas 2005, Volume 1: Temperature. S. Levitus, Ed. NOAA Atlas NESDIS 61, U.S. Govt Printing Off., Washington, D.C. 182pp.

Lutjerharms, J.R.E. & Roberts, H.R., 1988: The Natal Pulses; an extreme transient on the Agulhas Current. Journal of Geophysical Research, 93(C1): 631-645.

Lutjerharms, J.R.E., 2006: The Agulhas Current. Springer-Verlag, Heldeberg, xiii=329 p.

Manatsa, D., Morioka, Y., Behera, S.K., Matarira, C.H., Yamagata, T., 2013: Impact of Mascarene High variability on the East African 'short rains'. Climate Dynamics, [Online].

Marchesiello, P., McWilliams, J., & Shchepetkin, A., 2001: Open boundary conditions for long-term integration of regional oceanic models. Ocean Modelling, 3 (1-2), 1–20.

Marchesiello, P., Debreu, L. & Couvelard, X., 2009: Spurious diapycnal mixing in terrain- following coordinate models: The problem and a solution. Ocean Modelling., 26 (3-4), 156– 169.

Matano, R.P., Beier, E.J., & Strub, P.T., 2008: The seasonal variability of the circulation in the South Indian Ocean: model and observations. Journal of Marine Systems, 74, 315-328..

Meehl, G.A., Stocker, T.F., Collins, W.D., Friedlingstein, P., & others., 2007: Global climate projections. In: *the physical science basis*. Contribution of Working Group I to the Fourth Assessment Report of the Intergovernmental Panel on Climate Change. Cambridge University Press, Cambridge, p. 749–844

Meinen, C. S., & Watts, D. R., (2000), Vertical structure and transport on a transect across the North Atlantic Current near 42^0N: Time series and mean, Journal of Geophysical Research., 105(C9), 21,869–21,891.

Meyers, S.D., Kelly, B.G., & O'Brien, J.J., 1993: An introduction to wavelet analysis in oceanography and meteorology: With application to the dispersion of Yanai waves. Monthly Weather Review, 121, 2858-2866.

Moisan, J.R, and Niiler, P.P., 1998: The seasonal heat budget of the north Pacific: Net heat flux and heat storage rates (1950-1990). Journal of Physical Oceanography, 28 (1998), 1013-1038.

Morioka, Y., Tozuka, T., & Yamagata, T., 2010: Climate variability in the southern Indian Ocean as revealed by self-organizing maps. Climate Dynamics, 35:1059–1072

Morioka, Y., Tozuka, T., Masson, S., Terray P., Lou, J., & Yamagata, T., 2012: Subtropical Dipole Modes Simulated in a Coupled General Circulation Model. Journal of Climate, 25:1 140-155.

Nicholson, S. E., 1997: An analysis of the ENSO signal in the tropical Atlantic and western Indian Oceans. International Journal of Climatology, 345–375.

Penven, P., Lutjeharms, J. R. E., & Florenchie, P., 2006b: Madagascar: A pacemaker for the Agulhas Current system. Geophysical Research Letters, 33, L17 609.

Percival, D.B., & Walden, A.T, 1998: SPECTRAL ANALYSIS FOR PHYSICAL APPLICATIONS; Multitaper and Conventional Univariate Techniques, Cambridge University Press. The Pitt Building, Trumpington Street, Cambridge CB2 IRP, United Kingdom.

Qian, W., Hu, H., Deng, Y., & Tian, J., 2002: Signals of interannual and interdecadal variability of air-sea interaction in the basin-wide Indian Ocean. Atmosphere Ocean, 40, 293–311.

Rayner, N.A., Horton, E.B., Parker, D.E., Folland, C.K., & Hackett, R.B., Climate Research. Tech. Note74, UK Meteorological office, Bracknell, 1996.

Reason, C. J. C., 1999: Interannual warm and cool events in the subtropical mid-latitude south Indian Ocean region. Geophysical Research Letters, 26, 215–218.

Reason, C. J. C. & Mulenga, H., 1999: Relationships between South African rainfall and SST anomalies in the southwest Indian Ocean. International Journal of Climatology, 19, 1651–1673.

Reason, C.J.C., 2001: Subtropical Indian Ocean SST dipole events and southern African rainfall. Geophysical Research Letters, 28, 11, 2225-2227.

Reynolds, R. W., Rayner, N. A., Smith, T. M., Stokes, D. C. & Wang, W., 2002: An improved in situ and satellite SST analysis for climate. Journal of Climate, 15, 1609–1625.

Ridderinkhof, H., van der Werf, P.M., Ullgren, J.E., van Aken, H.M., van Leeuwen, P.J., de Ruitjer, W.P.M., 2010: Seasonal and interannual variability in the Mozambique Channel from moored current observations. Journal of Geophysical Research, 115, C06010.

Risien C.M., Reason, C.J.C., Shillington, F.A. & Chelton, D.B., 2004: Variability in satellite winds over the Benguela upwelling system during 1999-2000. Journal of Geophysical Research, 109,C03010.

Robinson, I.S., 2004: Measuring the Oceans from Space; The principles and methods of satellite oceanography. Praxis Publishing Ltd. Chichester, UK, 2004.

Rocha, A., & Simmonds, I., 1997b: Interannual variability if south–eastern African summer rainfall. Part 1: Relationships with air-sea interaction processes. International Journal of Climatology, 17, 235–265.

Rouault, M., White, S.A., Reason, C.J.C., Lutjerharms, J.R.E., Jobard, I., 2002: Ocea-Atmosphere Interaction in the Agulhas Current Region and a South African Extreme Weather Event. American Meteorological Society, 17, 655-669

Rouault, M., Lee-Thorp, A. M., & Lutjerharms, J. R. E., 2000: Observations of the atmospheric boundary layer above the Agulhas Current during along-current winds. Journal of Physical Oceanography, 30, 70–85.

Rouault, M., Pohl, B. and Penven, P., 2009: Coastal oceanic climate change and variability from 1982 to 2009 around South Africa. African Journal of Marine Science 2010, 32(2): 237-246.

Rouault, M.J. and Penven, P., 2011: New perspectives on Natal Pulses from satellite observations. Journal of Geophysical Research, 116, C07013.

Saji, N.H., Goswami, B.N., Vinayachandran, P.N., & Yamagata, T., 1999: A dipole mode in the tropical Indian Ocean. Nature 401: 360-363.

Shchepetkin, A. & McWilliams, J., 2005: The regional oceanic modeling system (ROMS): A split-explicit, free-surface, topography-following-coordinate oceanic model. Ocean Modelling, 9 (4), 347–404.

Snaith, H.M and Scharroo, R., 2011: Coastal Challenges for Altimeter Data, Dissemination and Services. In: *Coastal Altimetry*. S.Vignudelli, A. Kostinoy, P. Cipollini and J. Benveniste.

Stramma, L., & Lutjeharms, J. R. E., 1997: The flow field of the subtropical gyre of the South Indian Ocean. Journal of Geophysical Reseach, 102, 5513–5530.

Suzuki, R., Behera, S. K., Iizuka, S., & Yamagata, T., 2004: Indian Ocean subtropical dipole simulated using a coupled general circulation model. Journal of Geophysical Research, 109, C09001.

Torrence, C., & Compo, G.P., 1998: A practical guide to wavelet analysis. Bulletin of the American Meteorological Society, 79:61-78

van Seville, E., Beal, L. M. & Biastoch, A., 2010: Sea surface slope as a proxy for Agulhas Current strength, Geophysical Research Letters, 37, L09610.

Venegas, S.A., 2001: Statistical Methods for Signal Detection in Climate. Danish Center for Earth Systems Science (DCSS). Institute of Astronomy, Physics and Geophysics. University of Copenhagen, Denmark. DCSS Report #2

Venegas, S.A., Mysak, L.A. &. Straub, D.N., 1997: Atmosphere-ocean coupled variability in the South Atlantic. Journal of Climate, 10, 2094-2920.

Venzke, S., Latif, M. & Villwock, A., 2000: The Coupled GCM ECHO-2. Part II: Indian Ocean Response to ENSO. American Meteorological Society. 1371-1383

Wallace, J.M., Smith., C., Bretherton, C.S., 1992: Singular Value Decomposition of Wintertime Sea Surface Temperature and 500-mb Height Anomalies. Journal of Climate, 5, 561-576.

Walker, N. D., 1990: Links between South African summer rainfall and temperature variability of the Agulhas and Benguela current systems. Journal of Geophysical Research, 95, 3297–3319.

Washington, R., & Preston, A., 2006: Extreme wet years over southern Africa: Role of Indian Ocean sea surface temperatures. Journal of Geophysical Research 111: D15104, 1029/2005JD006724.

Xue, Y., Smith, T.M. & Reynolds, R.W., 2003: Interdecadal changes of 30-yr SST normals during 1871-2000. Journal of Climate, 16, 1601-1612.

Yu, L., & Rienecker, M. M., 1999: Mechanisms for the Indian Ocean warming during the 1997–98 El Nino. Geophysical Research Letters, 26, 735–738.